Design and Optimization of Novel Hybrid PLGA and Endosomolytic Polymer Nanoparticles for siRNA Delivery and Use as a Treatment for Osteoarthritis

By

Shubham Gulati

Thesis

Submitted to the Faculty of the

Graduate School of Vanderbilt University

in Fulfillment of the Requirements

for the Degree of

MASTER OF SCIENCE

in

Biomedical Engineering

May 13, 2022

Nashville, Tennessee

Approved:

Craig Duvall, Ph.D.

Johnathon Brunger, Ph.D.

Dedication

To my parents, Umesh and Shelly Gulati, for their constant support and unwavering love
and
To my sister, Pari Gulati, for being a constant source of joy and happiness

ACKNOWLEDGEMENTS

This work is a testament to the supportive, nurturing, kind, and intellectual individuals I have had the chance of learning from and working with during my time at Vanderbilt. I am truly grateful for my advisor, Dr. Craig Duvall. Thank you for believing in me as a first-year undergraduate student and allowing me to join the Advanced Therapeutics Laboratory. You have shaped my academic career and shown me what it means to be a scientist.

This thesis would not exist if it were not for my mentor, Carlisle DeJulius. Your work ethic and drive has been a constant source of inspiration. I am grateful for all that I have learned from you, and it is your dedication to the pursuit of science that will be my biggest lesson. Further, I could not have done this without the help of the rest of my fellow lab members. I would like to thank Shrusti Patel for her patience with me and her ability to always make the lab a place I wanted to come back to. To the rest of the lab members who were always there to chip in and teach me new skills, your help and support did not go unnoticed. Additionally, to my friends and peers who stuck with me throughout this experience, thank you!

Lastly, I would like to thank my family. My parents and sister have been a constant source of support and love. This work would not have been possible without your encouragement and willingness to help me through all of my problems.

List of Figures

Table of Contents

Chapter 1: Introduction and Significance

1.1 Motivation

Short interfering ribonucleic acids (siRNAs) offer immense potential for therapeutic activity due to their ability to silence gene expression with high specificity[1]. While three siRNA therapies have been approved by the US Food and Drug Administration (FDA), there are still limitations with regards to the delivery of siRNA[2]. The purpose of this project is to develop a novel polymer-based nanoparticle (NP) system for the delivery of siRNA that tackles existing limitations to the translation of this potent regulator of gene expression, particularly issues with stable delivery of siRNA to the cytosol of the intended cellular targets[3]. While this system is designed as a general platform, the application of this technology for osteoarthritis (OA) is discussed. OA is a debilitating disease of the joints and surrounding tissues without any disease-modifying OA drugs (DMOADs) approved for clinical use[4]. However, a variety of preclinical approaches seek to treat OA at a biological level[5]. A promising approach is the delivery of MMP13-specific siRNA (MMP13-siRNA) to the joint space[6–8]. Herein, we investigate the potential of our novel NP to act as a delivery vehicle for MMP13-siRNA in the joint space and target the progression of OA at a cellular level.

1.2 Innovation

Several approaches to developing NP systems for the delivery of siRNA have been attempted, including liposomes, exosomes, and polymer-based NPs[9]. Our lab previously developed pH-responsive polymer polyplexes (Ppxs) for the delivery of siRNA, giving the NPs the capability to disrupt the endosomal membrane and deliver their siRNA load while being trafficked intracellularly via the endosomal/lysosomal pathway[10–12]. However, the stability of

this system can be improved. Here, we propose the development of a novel hybrid endosmolytic polymer, dimethylaminoethyl methacrylate-co-butyl methacrylate (DMAEMA-co-BMA), and poly(lactic-co-glycolic acid) (PLGA) NP system for the delivery of siRNA, addressing existing issue with stability and activity of delivery vehicles. We further investigated the application of this NP design for the treatment of OA. Given, that there is no DMOAD on the market, this study provides an innovative approach to treating the biological underpinnings of OA. Our siRNA delivery system, if translated, could serve as a potential disease modifying drug for OA by slowing or arresting disease progression via interruption of cartilage breakdown by targeted silencing of MMP13.

1.3 Aims

The goal of this project is to generate a stable pH-responsive NP system for the delivery of siRNA and validate this system for the treatment of OA. This novel design consists of four distinct components: crystalline PLGA, endosmolytic DMAEMA-co-BMA (DB), coronal lipid-PEG, and target-specific siRNA. **The hypothesis for this novel NP design is that by varying the ratio of PLGA to DB and the DB polymer used, the stability, activity, and safety profile of this NP system can be optimized for intra-articular (IA) *in vivo* silencing of MMP13 to slow OA progression.** This work is pursued through the following 2 aims:

Aim 1: Optimize NP design for the delivery of siRNA by varying polymer composition

The first aim of this thesis is to better understand how varying the two core polymers that make up these NPs, PLGA and DB, impacts the properties of the NP system. A library of NPs is formulated by varying the endosomolytic polymer used ($DMAEMA_{50}$-co-BMA_{50} or $DMAEMA_{60}$-co-BMA_{40}) and varying the ratio of DB to PLGA (20%, 40%, 60% or 80%, wt:wt). These NPs are analyzed to better understand

how the composition impacts size, zeta potential, encapsulation efficiency, endosomal escape, cell toxicity, stability, and activity. After physical characterization, the NP library is tested to optimize for cytotoxicity and activity *in vitro* using the model gene luciferase. Experiments are also done to determine the endosomal escape abilities of this system, including visualization of cell uptake and endosomal escape in real time. Lastly, the dose responsive nature of the siRNA loaded NPs is studied to understand potency of this system.

Aim 2: Test the pharmacokinetics and pharmacodynamics of the optimized NP formulations in a murine model of OA

The second aim of this thesis is to test the optimized NP formulation for the delivery of MMP13-siRNA in a murine model of OA to determine the pharmacokinetic and pharmacodynamic effects of this disease modifying therapy. Following OA induction and single IA injection of the therapeutic, we analyze joint retention to understand the clearance rate of this NP. Further, pharmacodynamics is studied by analysis of the joint tissue to quantify how MMP13 expression levels were impacted by the treatment and by measurements of a functional pain outcome. These experiments provide a fundamental indication of the performance of this drug for the treatment of OA.

1.4 Outline

This thesis focuses on the development of a novel hybrid endosomolytic and PLGA polymer NP system for the delivery of siRNA and the use of this formulation as a DMOAD. Chapter 2 provides an overview of the use of nanoparticles and siRNA in drug design and background on the pathology of OA, existing treatments and clinical trials, and animal models currently used for research in this space. Chapter 3 discusses the optimization of the NP system

with a particular focus on the impacts varying the polymer composition has on general characteristics, stability, endosomal escape, and activity *in vitro*. Chapter 4 provides an analysis of the pharmacokinetics and pharmacodynamics of the optimized nanoparticle system to deliver MMP13-siRNA in a murine model of OA. Chapter 5 summarizes and discusses the impact of this work as a whole and considers future directions for this project and challenges for the treatment of OA in general. Each experimental chapter consists of a brief introductory section followed by the methods, results, and discussion.

Chapter 2: Background

2.1 siRNA as Therapeutics

The discovery of the ability of double-stranded RNAs (dsRNAs) to induce post-transcriptional gene silencing dates back to 1998 when Andrew Fire and Craig Mello were able to show this function in *Caenorhabditis elegans*[13]. They termed this capability RNA interference (RNAi). This led to an explosion in research showing the importance of non-coding RNAs for gene expression. In 2001, Elbashir and Caplen separately reported on the capability of short dsRNA strands, 21 and 22 nucleotides in length, to induce gene silencing in mammalian cells without nonspecific interferon responses[14,15]. These seminal publications identified the massive potential of siRNAs: the ability to inhibit gene expression with a simple nucleotide sequence.

Over the past twenty years, siRNAs have been extensively used to study gene function in biology. Further, the potential to treat previously "undruggable" diseases is vast: unlike most small molecule drugs, siRNAs do not rely on the ability to bind proteins. The possibilities of siRNAs as therapeutics has led to immense interest from drug developers and the formation of several companies[16–18]. The therapeutic potential of siRNA is immense, with possible applications ranging from the treatment of viral infections[19,20], hereditary disorders[21], and cancer[22,23]. By 2013, at least 22 RNAi-based drugs had entered clinical trials[3].

However, there have been several snags along the road to translation, from failed clinical trials[24,25] to divestment from the RNAi space by major pharmaceutical companies over concerns regarding the success of siRNA[26]. Despite these setbacks, continued research led to improvements siRNA design and production[27] and in 2018, the FDA approved the first siRNA therapeutic, patisiran, for the treatment of hereditary transthyretin amyloidosis with

polyneuropathy[28]. Currently, three siRNA therapeutics are on the market[2]. Even with these recent accomplishments, there are still limitations with regards to the translation of siRNA[27].

2.1.1 siRNA mechanism of action

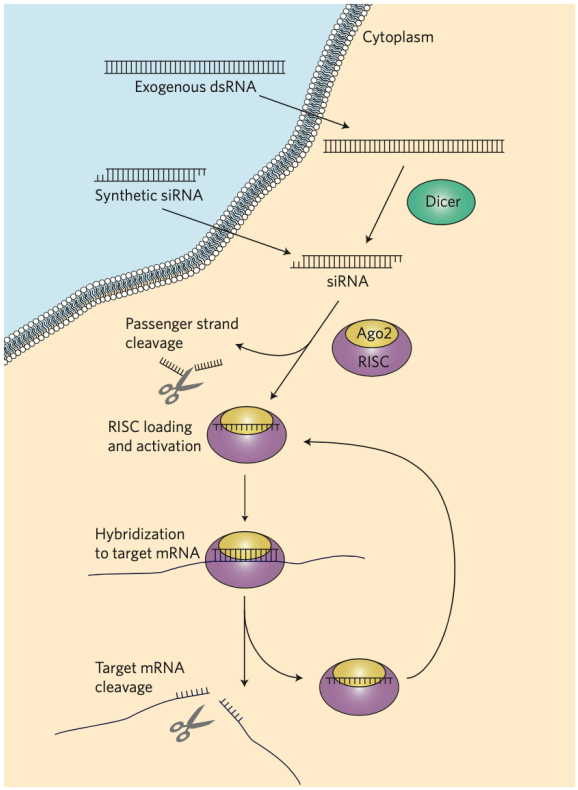

Figure 1. The mechanism of RNAi with exogenously delivered dsRNA or synthetic siRNA. *Kanasty, R., Dorkin, J. R., Vegas, A. & Anderson, D. Delivery materials for siRNA therapeutics.*

The mechanism of action of siRNA has been extensively studied. Exogenously delivered dsRNA is first cleaved via endonucleolytic processing by the ribonuclease Dicer, resulting in the production of siRNA[29]. These siRNAs are ~21-25 nucleotides in length with 2-nucleotide, single-stranded overhangs on the 3' ends and monophosphate groups on the 5' ends[30–34]. Synthetic siRNA is designed to mimic this output. siRNA is then recognized by the RNA-induced Silencing Complex (RISC), which contains the Argonaute (AGO) protein[35]. In particular, AGO2 has been identified for siRNA-mediated silencing in humans[36]. AGO2 serves to separate the two strands of the siRNA, tethering the guide siRNA and cleaving the passenger

strand[29]. The activated RISC complex then undergoes several cycles in order to identify mRNA segments that are complementary to the guide strand, followed by cleavage and release of the mRNA strand[37]. Thus, translation of the mRNA strand is prevented and silencing of gene expression is achieved with high specificity (**Figure 1**).

2.1.2 Clinical applications

The ability to specifically knock-down the expression of a gene endows siRNA with great potential for clinical translation. For this reason, the use of siRNA has been studied for a breadth of conditions, and three drugs have already been approved by the FDA with another seven candidates currently in Phase 3 clinical trials[2]. The first three FDA-approved therapies, patisiran[28], givosiran[38], and lumasiran[39], all of which are produced by Alnylam Pharmaceuticals, treat genetic disorders affecting the liver. Though liver targeting represents "low-hanging fruit" due to its role in processing metabolites, target organs have since expanded past the liver[2]. For example, inclisiran treats hypercholesterolemia[40], and fitusiran treats hemophilia A and B[41]. The market for investing in the development of siRNA therapeutics for the clinic remains high. Patisiran generated $166.4 million in revenue in 2019[2] and Givosiran is projected to generate $560 million in sales by 2025[42].

2.1.3 Limitations

The main challenge to the translation of siRNAs to the clinic is effective delivery of the siRNA to its site of action (**Figure 2**), namely the cytosol of cells in the target tissue/organ[43]. The broad issue of delivery can be divided into several stages. For systemically delivered siRNAs, the first hurdle is reaching the target site. Once arrived, either through systemic circulation or local administration, the therapeutic must be taken up by cells. Finally, the siRNA must be

delivered to the cytosol to be available for RISC loading. At each of these steps, the siRNA is faced with the possibility of clearance and/or degradation[3].

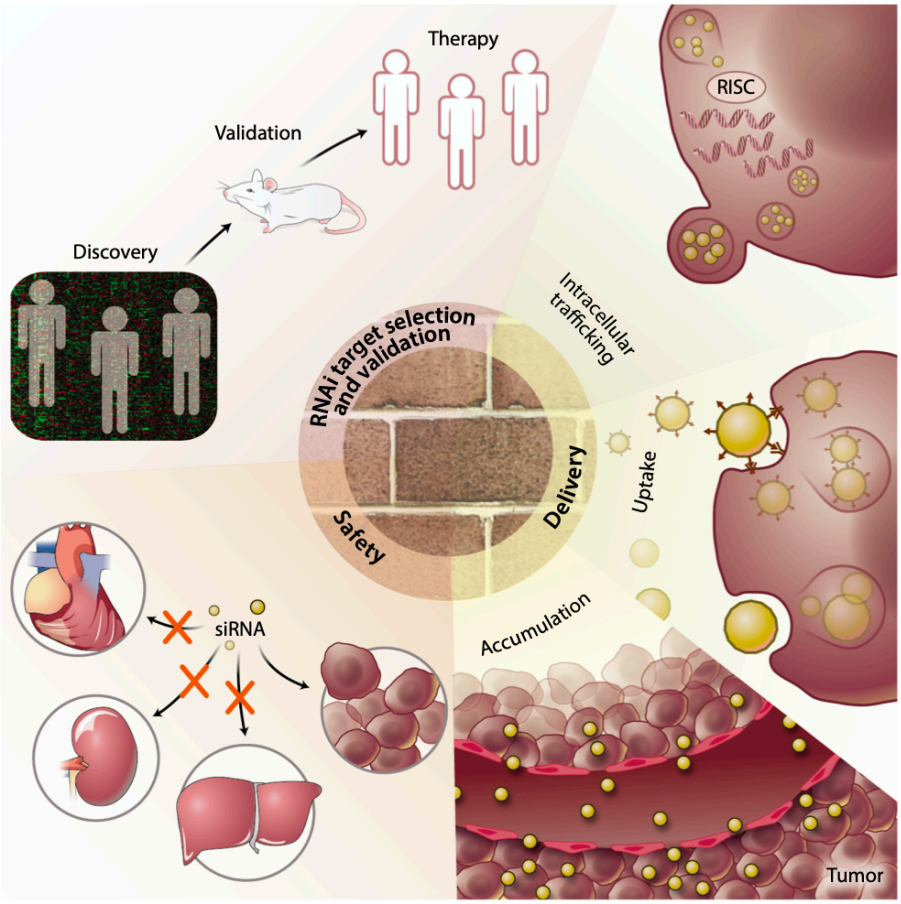

Figure 2. Limitations and factors to consider in the design and use of siRNA delivery vehicles. *Wu, S. Y., Lopez-Berestein, G., Calin, G. A. & Sood, A. K. RNAi therapies: drugging the undruggable.*

When delivered systemically, free siRNA is vulnerable to degradation by serum nucleases and non-specific interactions with serum proteins and non-target cells[44]. Even when encapsulated by delivery vehicles, the drug is subject to serum protein adsorption, which leads to uptake by the reticuloendothelial system and clearance by immune cells[45]. Further, siRNA must avoid renal clearance. siRNA will often exit the bloodstream via the kidneys, leading to elimination via the urine[46]. The combination of renal clearance and degradation by nucleases leads to a short half-life, with studies suggesting plasma half-lives of five minutes to one

hour[47,48]. These issues with target-site accumulation make it difficult to achieve therapeutic dose levels at the site of interest[1].

If the siRNA avoids degradation and renal clearance, it must traverse the endothelial cell lining to enter the tissue of interest. This poses further difficulty since the number of adherence and tight junctions prevent travel of the siRNA into the tissue[2]. For this reason, siRNA uptake is most commonly observed in tissues with discontinuous endothelia, like the liver, or in tumor tissue with leaky vasculature[3]. Organs with tight vasculature are more difficult to treat with siRNA[49], and is why siRNA has often been considered optimal for targeting hepatocytes or cancer cells.

Once present at the tissue of interest, the siRNA must be taken up by the target cells. However, due to their negative charge and relatively large size, siRNAs are unable to spontaneously cross the cell membrane via passive diffusion[50]. Therefore, siRNA is typically internalized via endocytosis. However, during endosomal trafficking, siRNA is subject to degradation or recycling back to the extracellular space[51]. To achieve cytosolic delivery, the siRNA must escape the endosome[9]. Finally, once in the cytosol, the siRNA must be recognizable by the RISC complex for successful gene silencing. To ensure that there are no issues with recognition of the siRNA, the 5' end of the guide strand is often left unaltered[52].

Along with these difficulties in delivery, there is the possibility of an immunogenic response. Exogenously delivered siRNA can be falsely recognized by the immune system as viral RNA molecules[53]. siRNAs have been found to activate interferon responses, causing cell death[54], along with Toll-like receptors (TLRs)[55], causing adverse immune reactions[56]. These immune responses and the possibility of toxicity pose further concerns with regards to the translation of siRNA therapeutics.

2.2 Addressing the Limitations of siRNA

In order to address the numerous limitations associated with the delivery of siRNA, two broad approaches have been used. One approach is to chemically modify the siRNA structure itself[57]. The other is to use delivery vehicles for siRNA[27,43]. Both approaches aim to improve the stability of the siRNA, prevent degradation, retain function, and reduce immune responses. Overall, these approaches modulate the pharmacokinetics and pharmacodynamics of siRNA therapeutics, improving their safety profiles and increasing efficacy.

2.2.1 Chemical Modifications to siRNA

siRNA molecules can be chemically modified at the sequence or structural level to increase stability and reduce immunogenicity, while preserving silencing activity[58,59,57]. siRNAs are double stranded nucleotide sequences, with each strand consisting of nucleotides on a sugar backbone linked by phosphodiester bonds. To retain function, certain moieties must be retained, particularly the free hydroxyl and phosphate group at the 5' end of the sense strand[60]. However, to some extent, the sugar-phosphate backbone, along with the purine and pyrimidine bases, are free to be modified.

One of the most commonly utilized and earliest modification of siRNAs is replacing the unstable phosphodiester backbone with a phosphorothioate (PS) backbone[61]. This modification consists of replacing the non-bridge oxygen atom on the phosphate backbone with a sulfur and leads to a decrease in recognition by nucleases and phosphodiesterases[62]. Further, this modification makes the siRNA more hydrophobic, increasing binding to plasma protein carriers and subsequently improving uptake by cells [63]. This modification of the PS backbone improves stability and efficacy of free siRNA, making it one of the most important and successful modifications in the field[43,49]. However, overuse of this modification can be problematic. Studies

show that the use of PS modifications throughout the length of the siRNA leads to decreased activity and even cytotoxicity, most likely due to issues with RISC recognition[64]. Partially PS-modified siRNA molecules have proved ideal. In particular, use of PS modification at both the 3' and 5' ends of the strand have demonstrated similar efficacy to unmodified strands while improving pharmacokinetics[65].

The ribosugars of siRNA are also targets for modification. This is most commonly performed at the 2' position, since the 2'-OH group is not necessary for activity of the siRNA[49]. Further, the 2'-OH groups participate in nuclease-mediated cleavage of the siRNA, making modification of this portion a logical approach for reducing endoribonuclease degradation and increasing stability[66]. The most common modifications to the ribose sugar consist of substituting the 2'-OH with a fluorine, O-methyl group, or O-methoxyethyl group, resulting in 2'-F, 2'-OMe, or 2'-MOE, respectively. The 2'-F and 2'-OMe modification have been found to further reduce the immunogenicity and immune-mediated off-target effects of siRNA by reducing immune recognition by TLRs[60]. Also, the 2'-OMe modification has been found to inhibit the production of TNF-alpha that is induced by unmodified sugars within the siRNA[67].

While ribosugar modifications show promise, excessive use can be detrimental, similar to the case of PS-modification. Extensive sugar modification causes off-target effects, reduces RNAi activity, and can even lead to the production of toxic metabolites following degradation[68,69]. Modifying sugars of both strands of the siRNA duplex with 2'-OMe moieties causes a reduction in activity. Alternatively, 2'-OMe modification of only the sense strand leaves silencing intact if the "seed" region of the siRNA remains unmodified[70]. Another strategy is alternating 2' substitutions like 2'-F and 2'-OMe to increase nuclease resistance and retain gene silencing[49].

Given the success of these siRNA modifications, most of the currently FDA-approved and late-stage siRNA drugs utilize a combination of PS and 2'-OMe and 2'-F modifications[2]. For this reason, we also use these modifications in the design of our siRNA to provide protection against endo- and exonucleases and increase silencing efficacy[71,72]. Our siRNAs are chemically modified with an alternating 2'-F and 2'-OMe "zipper" pattern and PS bonds on the ends of each siRNA strand[73,74]. Preliminary data from our laboratory has shown that siRNA with these modifications had higher *in vitro* activity and stability in comparison to the unmodified siRNA.

Modifications of siRNA are not only limited to improving bioavailability but can also be used for research purposes. Fluorescent molecules can be covalently attached to siRNA molecules in order to study biodistribution of the therapeutic and cellular uptake[1]. Within this work, siRNAs with covalently bound Cy5, rhodamine, and Black Hole Quencher are used to characterize the delivery, retention, and release profile of siRNA.

2.2.2 siRNA Delivery Enhancers

Delivery enhancers are a useful means of addressing the pharmacokinetic and cellular uptake issues faced by free siRNA. Though chemical modification can improve its stability, their 13-14 kDa size allows for high renal clearance. Additionally, the charged and hydrophilic nature of siRNA prevents them from crossing the lipophilic cell membrane via passive transport[2]. Two major classes of delivery enhancers addressing these issues are covalently bound ligands and nanocarriers for siRNA.

In order to improve pharmacokinetic properties, increase transport across the cell membrane, and even target specific cells, siRNA can be covalently bound to moieties like cholesterol, folate, various peptides, and aptamers[75,76]. These covalent modifications work via different methods. For example, conjugation with cholesterol can lead to improved systemic

circulation by increasing binding of the siRNA to albumin and inducing cellular uptake via gymnosis[77]. On the other hand, bioconjugates use cell-specific targeting ligands, like targeting peptides or antibodies, to enhance delivery and uptake of siRNA by increasing delivery to a particular subset of cells[78]. One example is the conjugation of siRNA with glycoproteins terminating with N-acetylgalactosamine (GalNAc). GalNAc show a high binding affinity and specificity to asialoglycoprotein (ASGPR), which is a receptor that is highly expressed in hepatocytes[79]. Triantennary GalNAc (tri-GalNAc) has been conjugated to siRNA, resulting in specific delivery and internalization of siRNA by hepatocytes[80]. The use of GalNAc as a bioconjugate has shown clinical success as well, with both givosiran and lumasiran being approved by the FDA[81]. These successes have made the use of GalNAc popular for the hepatic delivery of siRNA. Approximately 66% of RNAi drugs in clinical trials are GalNAc conjugates[27]. There is a variety of conjugates besides GalNAc being investigated for siRNA delivery; in general, these conjugates exhibit less toxicity and immunogenicity compared to nanocarriers because of their smaller size[66]. The success of bioconjugates in clinical trials indicates the promise of this strategy to enhance the targeted delivery of siRNA.

Another option to address the challenges of systemic circulation, tissue penetration, cellular uptake, and endosomal escape is the use of nanocarriers[82], which includes lipid NPs (LNPs)[83], polymeric NPs[84,85], exosomes[86,87], nucleic acid nanostructures[88], and many more[89]. While each has their own various benefits and drawbacks, LNPs and polymeric systems will be briefly discussed here. The most extensively studied and successful nanostructure to date for the delivery of siRNA are LNPs, which are used in the formulation of patisiran, the first siRNA drug to receive FDA approval[90]. LNPs for siRNA delivery are composed of cationic or ionizable lipids and are approximately 100 nm in diameter. This design is intended to promote RNA

packing with the use of complementarily charged lipids, increase stability by providing protection from degradation, and allow for transport across the cellular lipid bilayer[91]. LNPs are often also PEGylated in order to avoid aggregation, opsonization, and clearance via the reticuloendothelial system[49]. LNP packaging helps prevent siRNA from degradation and improves pharmacokinetics and bioavailability, decreasing the effective dose of siRNA needed for efficacy[90]. However, LNPs also have their limitations, particularly by triggering adverse immune responses. For this reason, patisiran requires premedication with steroids and antihistamines to avoid or suppress this possibility[92].

Polymeric nanoparticles are promising because of the ability to tune their structure, surface charge, and composition in order to optimize stability, delivery, and encapsulation of siRNA[9]. While there are numerous polymers available, biodegradable, biocompatible, and non-toxic polymers are the most attractive for these delivery vehicles: this include chitosan, cyclodextrin, polyethyleneimine (PEI), and poly(lactic-co-glycolic) acid (PLGA)[1,93]. Chitosan is a natural cationic polymer and has been used extensively due to its positive charge encouraging loading of negatively charged siRNA[94]. The charge ratio of these two components can be tuned by adjusting the ratio of amines to phosphates (N:P) to optimize siRNA encapsulation[95]. Cyclodextrin-based polycations (CDPs) are another set of polymers that have been used for the delivery of siRNAs. Again, the cationic structure complexes with siRNA duplexes, and further, the cyclodextrin molecules allow for modification of the corona through linkages with functionalized adamantane molecules[1]. Adamantane functionalized with transferrin and PEG have been used to increase cell targeting and reduce clearance and have shown efficacy for the silencing of oncoproteins in non-human primates[96]. PEI has also been used as a delivery vehicle, offering unique benefits in addition to its cationic charge. The extensive dense branching of PEI

condenses siRNA, providing protection from degradation by RNases[97]. Further, its ability to act as proton sponge buffers the acidic inner compartment of an endosome, resulting in endosomal escape and delivery of siRNA to the cytosol[1]. Again, PEGylation has been combined with these polymeric nanocarriers, like PEI, to reduce toxicity[98]. Finally, PLGA is an FDA-approved, biocompatible, and hydrolytically degradable polymer that is commonly used for nanoparticles and allows for the controlled and sustained release of siRNA[99]. PLGA proves interesting because of the ability to extensively modify the surface of these NPs, allowing for enhanced targeting and cellular uptake[100,101].

2.3 OA and Clinical Approaches

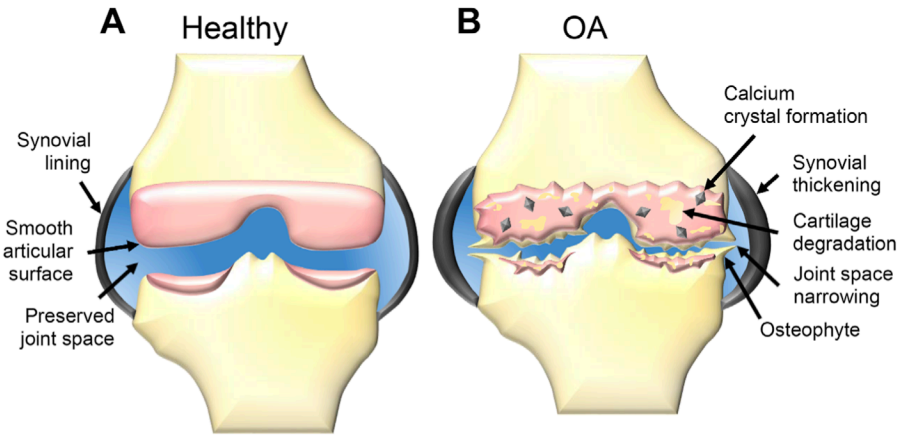

Figure 3. Pathology of (**A**) a healthy knee joint and (**B**) a knee joint afflicted with OA. *DeJulius, C. R., Gulati, S., Hasty, K. A., Crofford, L. J. & Duvall, C. L. Recent Advances in Clinical Translation of Intra-Articular Osteoarthritis Drug Delivery Systems.*

OA is a chronic degenerative disease affecting joints and their surrounding tissues, causing pain and loss of mobility. It presents with degradation of cartilage, joint inflammation, osteophyte formation, synovial thickening, and articular calcium crystal deposition[102] (**Figure 3**). Further, the disease is extremely prevalent, affecting more than 25% of people over the age of 45, and the prevalence is expected to rise with an aging population[103]. This widespread nature is most likely because OA is associated with a variety of conditions including mechanical and

biochemical factors[104], joint misalignment/injury[105], obesity[106], genetic disposition[107], and aging[108]. Despite this prevalence, the molecular events that cause this disease remain unknown. OA is classified into two major categories: primary OA, which arises from unknown causes (idiopathic), and secondary OA, which is due to an identifiable event like injury, disease, or infection. A common form of secondary OA is post-traumatic OA (PTOA), which follows an injury. This makes PTOA common among athletes and individuals with labor intensive careers and leads to surgical interventions 7-9 years earlier than with primary OA[109]. PTOA makes up ~12% of all US OA cases but causes a high loss in quality of life due to its occurrence at an early age[110]. Additionally, OA poses a substantial financial cost on the US healthcare system with a price point of over $44 billion annually[103]. The immense human and monetary cost of OA creates a pressing need for treatments.

2.3.1 OA Treatments

Even today, the best interventions to control OA remain weight loss and exercise; however, patient compliance is low. Surgical options exist but are typically reserved as a last resort. These procedures include arthroscopic lavage, microfracture[4], and total joint arthroplasty[111]. While invasive procedures like total joint arthroplasty are effective, the financial cost posed by these operations is a major motivation for the development of pharmaceutical treatments[112]. However, current pharmaceutical approaches are only palliative, and there are no clinically approved disease modifying OA drugs (DMOADs).

Current pharmaceutical drugs for OA treat pain, and the first line of treatment is topical[113] or oral[114] non-steroidal anti-inflammatory drugs (NSAIDs). These approaches offer marginal pain relief; however, oral delivery, which proves the most effective, is limited by gastrointestinal complications[115]. Further, NSAIDs do nothing to reduce cartilage degradation.

Another limitation posed by these systemic drugs is limited accumulation IA. For this reason, local injection has been explored to increase bioavailability in the joint and reduce systemic toxicity[116]. One approach is the injection of hyaluronic acid (HA) to provide temporary cushioning of affected joints[117]. Another approach, which is recommended by the Osteoarthritis Research Society International (OARSI) and the American College of Rheumatology, is the delivery of corticosteroid via IA injection to aid symptomatic joints[118]. While there are five FDA-approved corticosteroids for OA, these approaches still only provide temporary pain relief, leave the underlying issue unaddressed, and are not sustainable for long-term management due to extensive side effects[119]. In particular, long-term corticosteroid use has demonstrated chondrotoxicity[120] and loss of cartilage volume[121]. Further, these IA approaches are subject to rapid clearance from the joint space. Small molecules are cleared through the synovial vasculature while macromolecules are drained through the lymphatics[116]. This results in poor pharmacokinetics, with half-lives ranging from 1-4 hours for NSAIDs and corticosteroids and ~1 day for large molecular weight HA[122].

Several drug delivery systems have been investigated to treat OA and address the aforementioned issues. Despite extensive research and promising preclinical studies, only six drugs have shown promise in the clinic. These include three HA hydrogels, two polymeric microparticles, and one liposomal formulation, all of which have been reviewed extensively[5]. However, these systems are still limited by their focus on pain relief. Therefore, DMOADs are needed to actively target the underlying mechanisms causing OA at a molecular level and improvements upon the pharmacokinetics and pharmacodynamics of drug delivery systems are necessary for clinical translation of any solution.

2.3.2 Silencing MMPs for OA Treatment

While the exact method of OA progression is not understood, it is evident that early stages of mechanical stress lead to the disturbance of the extracellular matrix (ECM), stimulating synoviocytes and chondrocytes to produce inflammatory cytokines and catabolic enzymes including matrix metalloproteinases (MMPs)[123] (**Figure 4**). In a feed-forward cycle, damage to the IA surfaces increases exposure of type II collagen fibrils to MMPs, leading to further degradation deeper into the cartilage layers[124]. Combined with increased friction, this causes chondrocyte loss and exposure of subchondral bone. Degradation products of type II collagen activate synovial macrophages, furthering this cycle[125,126]. In addition, several upstream mediators of arthritis, including interleukin-1beta, Wnt, c-Jun N-terminal kinase, and reactive oxygen species, independently increase MMP expression. Therefore, approaches targeting reductions in MMP expression can prove to be effective DMOADs for the treatment of OA[127].

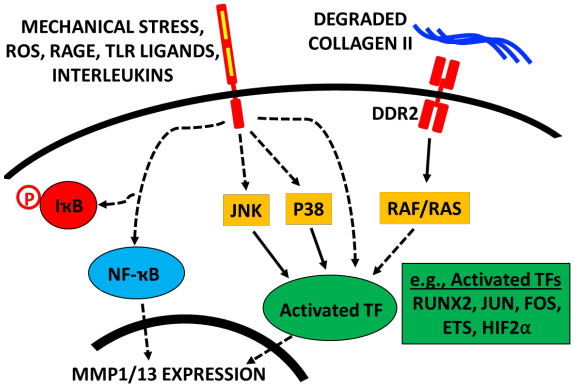

Figure 4. Biochemical and mechanical stimuli that result in the activation of MMP1/13 expression.

Non-selective inhibitors of MMPs have previously made it to clinical trials for the treatment of cancer, but systemic delivery was faced with complications due to the disruption of normal tissue homeostasis[128]. However, the use of specific MMP inhibitors and IA delivery can address these issues and possibly produce a disease modifying treatment for OA. MMP13 has been identified as a key proteolytic driver of cartilage loss in OA, making it an ideal candidate

for inhibition[6]. Previous studies have shown that this is an effective strategy, with the use of a MMP13 specific inhibitor reducing cartilage lesion severity and aggrecan degradation in a PTOA animal model[129]. While promising, small molecule inhibitors of this nature face issues with specificity due to shared domains of the collagenases and the homology of MMP catalytic sites[130]. Further, even though improvements in OA pathology have been observed with small molecule MMP inhibitors, treatments face issues with nephrotoxicity due to off-target effects[131]. For these reasons, the use and delivery of RNAi to the joint may prove to be an optimal alternative for silencing MMP13 activity and treating OA.

Chapter 3: Optimization of Hybrid PLGA and Endosomolytic Polymer Nanoparticles: *In vitro studies*

3.1 Introduction

The delivery of siRNA poses a major difficulty for translation[9]. siRNA is readily degraded if delivered freely and shows poor transfection capabilities. There is great need for a delivery system in order to take advantage of the potent regulation of targeted gene expression that siRNA therapeutics offer. Nanoparticles have emerged as an ideal delivery vehicle for siRNA[3]. However, there are several issues with NP systems as well. Particles must be stable enough to circulate through the blood stream or be retained when locally delivered and be taken up by cells in the target tissue. Further, siRNA must be delivered to the cytosol, which requires that NPs disrupt the endosomal membrane during endosomal/lysosomal trafficking. While our lab and several others have proposed NP systems for the delivery of siRNA, all have limitations with regards to either stability, siRNA delivery, or retention[2]. These limitations have clear impacts on the efficacy of the systems.

Our lab has previously published on the use of PEG conjugated with the pH responsive and endosomolytic polymer DMAEMA-co-BMA for the formation of siRNA loaded Ppxs. These nanoscale Ppxs showed promise with their ability to transfect cells *in vitro* and *in vivo*[11,12,132]. However, data indicated that the conjugation of PEG with DB led to reduced activity of the DB polymer's endosomal escape ability[12]. Further, these Ppxs offered room for improvement with regards to stability.

Rather than a Ppx approach, herein we propose the design of an innovative NP that consists of three distinct polymer components: lipid-PEG, DMAEMA-co-BMA, and PLGA (**Figure 5**). Free DB was used for its ability to complex with siRNA, enhancing loading

efficiency, and its pH responsive characteristics that allow for endosomal escape[10]. PLGA (50:50 L:G) was incorporated to increase the stability of the NPs by adding crystallinity to the NP polymer core and to provide shielding from DB toxicity. 1,2-distearoyll-sn-gglycero-3-phophoethanolaamine-N-[methoxy(polyethyllenee glycol)-5000] (ammonium salt) (DSPE-PEG or Lipid-PEG) was used to coat the polymers to ensure that these NPs were biocompatible. Further, this design makes the outer coating modular, allowing for future alterations to the NP surface chemistry to enhance cell targeting or improve bioadhesion. In order to optimize this novel design, we tested two different DB polymers and four ratios of DB to PLGA for the core of the polymer. This resulted in a library of eight NPs.

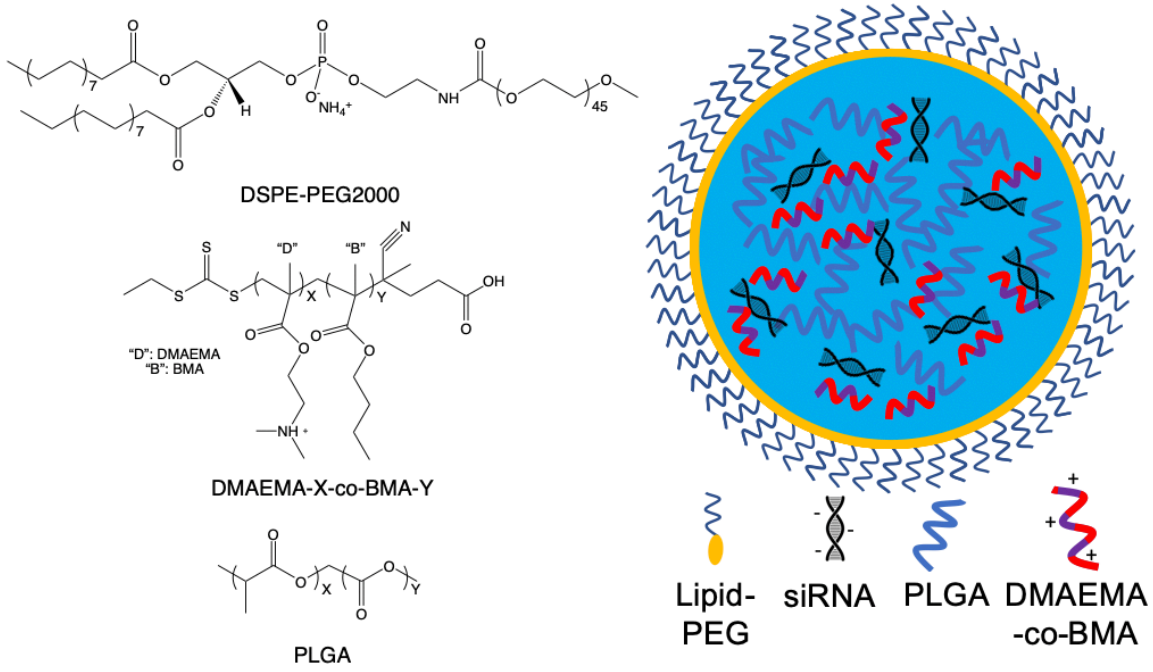

Figure 5. Design of a hybrid PLGA and endosomolytic polymer NP for siRNA delivery. (**A**) Polymer components of the NP. For DMAEMA-co-BMA the DMAEMA:BMA ratio (X:Y) was either 60:40 or 50:50. For PLGA the lactide:glycolide ratio (X:Y) was 50:50. (**B**) The siRNA loaded nanoparticle consists of a PLGA and DMAEMA-BMA core with a Lipid-PEG corona.

Overall, the goal of this design is to create NPs that have high siRNA loading efficiency, are stable *in vivo*, and are able to deliver siRNA to the cells via a pH-responsive endosomal escape mechanism. The library of NPs was characterized for size and charge, followed by activity, stability, and cellular uptake.

3.2 Materials and Methods

Materials

All materials were purchased from Sigma-Aldrich unless otherwise stated. PLGA 50:50 (Resomer RG 503) with a molecular weight (Mw) of 24,000-38,000 was used for the formulation of the nanoparticles. DMAEMA and BMA were purified of inhibitors with an activated aluminum oxide column. Lipid-PEG was purchased from Avanti Polar Lipids.

siRNA Preparation

siRNA was synthesized inhouse using a MerMade 12 Oligonucleotide Synthesizer (Bioautomation Corportation). Luciferase specific siRNA (Luc-siRNA) was synthesized with the following sense and antisense sequence respectively, fC*mA*fA mU fU mG fC mA fC mU fG mA fU mA fA mU fG*mA*fA and 5PHO mU*fU*mC fA mU fU mA fU mC fA mG fU mG fC mA fA mU*fU*mG. A scrambled siRNA (Scr-siRNA) was also synthesized with the sense and antisense as follows: fC*mG*fU mU fA mA fU mC fG mC fG mU fA mU fA mA fU*mA*fC and v5PHO mG*fU*mA fU mU fA mU fA mC fG mC fG mA fU mU fA mA*fC*mG, respectively. Scr-siRNA labeled with Cy5, TAMRA, and Black Hole Quencher 2 (BHQ2) were also synthesized.

DMAEMA-co-BMA Synthesis

DMAEMA-co-BMA (DB) was synthesized at D:B ratios of 50:50 and 60:40 via a RAFT controlled polymerization according to previously published methods[10].

Nanoparticle Formulation

The nanoparticles (NP) were formulated using an oil-in-water (O/W) nanoprecipitation. DMAEMA-60-co-BMA-40 (40B) or DMAEMA-50-co-BMA-50 (50B) were co-dissolved with varying amounts of PLGA, either 20%, 40%, 60%, or 80% by mass, in acetonitrile. The aqueous phase consisted of 20% DSPE-PEG by mass of total polymer dissolved in water. These dissolutions resulted in an aqueous phase that was 50x the volume of the organic phase. siRNA was added to the organic phase immediately prior to the combination of the two solutions. Luc-siRNA or a Scr-siRNA was used for these formulations. The organic phase was slowly added through a syringe into the stirring aqueous solution, resulting in a cloudy suspension. A 10:1 mole ratio of protonated amine from the DMAEMA units to negatively charged phosphate from the siRNA (N^+:P^-) was used to calculate the amount of DB and siRNA used in these formulations based on this equation:

$$\text{nmol polymer} = \frac{(\text{nmol siRNA}) * (\text{charge siRNA})(\text{N: P ratio})}{(\text{charge polymer})}$$

The resulting NP suspension from the O/W emulsion was concentrated in Amicon 30k 15mL spin filter tubes (MilliporeSigma) by spinning down at 1000xg until concentrated ~25 times, about five minutes (Centrifuge 5804, Eppendorf). The remaining solution was resuspended in a 270 mM sucrose solution to the initial volume prior to spinning, and then spun down to concentrate ~50x. This resulting NP solution was resuspended, aliquoted, and flash-frozen for storage at -20°C.

PEG-DB Ppx Formation

PEG conjugated to DMAEMA-50-co-BMA-50 (PEG-DB) Ppxs were used as controls and the polymers and Ppxs were prepared as described in previously published methods[12]. The PEG-DB was synthesized by first synthesizing PEG conjugated to ECT, a chain transfer agent.

ECT was coupled to 5 kDa or 20 kDa PEG (JenKem) via a diicylcohexyl carbodiimide (DCC) 4-dimethylaminopyridine (DMAP) coupling reaction and then purified. DMAEMA-co-BMA was then RAFT polymerized off of these polymers at a 50:50 mol ratio of DMEMA to BMA using AIBN as an initiator, described in previous publications[11]. The resulting polymers were used for Ppx formation. PEG-DB was complexed with siRNA and used to form Ppxs as described in previously published methods[12]. This resulted in both 5k PEG-DB and 20k PEG-DB Ppxs as controls.

Encapsulation Efficiency of Nanoparticles

NP siRNA encapsulation was quantified via a Quant-iT Ribogreen assay kit (ThermoFisher). Assay reagents were prepared as suggested by the manufacturer, and Ribogreen fluorescence intensity was measured at 520 nm after excitation at 480 nm with a fluorescence plate reader (Tean Infinite F500). The NP suspension prior to spin filtering was used in this assay. The fluorescence intensity of the NP groups was compared against a standard curve generated with siRNA-only controls and used to calculate the encapsulation efficiency of the different NPs.

Size and Charge of Nanoparticles

Nanoparticle hydrodynamic diameter and charge were measured via dynamic light scattering (Zetasizer Nano ZS, Malvern Instruments). These measurements were done on 100 nM, based on siRNA content, suspensions of NPs.

Hemolysis Assay

A red blood cell (RBC) hemolysis assay was performed based on previously described methods[133]. Blood was drawn from consenting human donors following an IRB-approved protocol. RBCs were isolated and resuspended in a saline solution. Wells were plated with NPs

or free DB co-polymers and buffer solutions of pH 5.6, 6.2, 6.8, and 7.4 and allowed to incubated for 30 minutes. For the negative control a saline solution with the same amount of sucrose as the NP treatments was created and for the positive control a 20% Triton-X solution, which induced complete RBC lysis, was used. The RBC suspension was then added to each well such that each well had a final polymer concentration of 40 ug/mL and incubated for another 30 minutes. The plates were then centrifuged and the supernatants were isolated and analyzed for absorbance at 450 nm using a plate reader. The percent hemolysis due to each NP at each pH was calculated by subtracting background RBC absorbance, as identified by the negative control, and dividing by the relative absorbance of the positive control.

Cell Culture

All cells used in these experiments were cultured with Dulbecco's modified eagle's medium (DMEM, Gibco Cell Culture), containing 4.5 g/L glucose and supplemented with 10% FBS (Gibco Cell Culture), and 1% Penicillin-Streptomycin (Gibco Cell Culture). MDA-MB-231, human epithelial breast cancer cells, were transfected with lentivirus encoding firefly luciferase (Luc-MDA-MB-231), as described in a previous publication[12]. MDA-MB-231 cells were also transfected with Gal8-yfp as previously described (Gal8-MDA-MB-231)[134]. Cell cultures were maintained on 75 cm^2 polystyrene tissue culture flasks (BD Biosciences) and grown to ~90% confluency before harvest and passage. All cell cultures were maintained in sterile incubators at 37°C with a humidified 5% CO_2 atmosphere.

Cell Viability

Luc-MDA-MB-231 cells were seeded in a black-walled 96-well plate at 4,000 cells/well. After 24 hr, the media was replaced and cells were treated with varying siRNA doses of the NP library (0 nM–100 nM). After 24hrs, the media containing the NPs was replaced with fresh

media. After another 24hrs, the cell viability was determined via the CellTiter-Glo luminescent cell viability assay (Promega, Madison, Wisconsin). CellTiter-Glo reagents were prepared and used to treat cells based on manufacturer recommendations. The luminescence was measured using an IVIS Lumina III imaging system (Caliper Life Sciences, Hopkinton, Massachusetts). Cell viability was compared against untreated control groups.

In Vitro Luciferase Silencing of MDA-MB-231 Cells

Luc-MDA-MB-231 cells were seeded in a black-walled 96-well plate at 4,000 cells/well. After 24 hr, the media was replaced and cells were treated with varying siRNA doses of the NP library (0 nM–100 nM) in triplicate. After 24hrs, the media containing the NPs was replaced with fresh media. After another 24hrs, media containing luciferin substrate (150 ug/mL) was added to the wells and the bioluminescence was measured using an IVIS Lumina III imaging system. For the analysis of knockdown, all data was normalized to NPs loaded with scrambled siRNA, accounting for nonspecific toxicity.

Galactin8 Assay

Gal8-MDA-MB-231 cells were plated in a black-walled glass-bottom 384 well plate (Greiner) at a density of 750 cells per well and allowed to adhere overnight. After 24 hrs, cells were treated with 50 nM or 12.5 nM doses of the 50B NP library loaded with Cy5 siRNA with eight replicates for each group. Each well was imaged approximately every 80 min over a period of 24 hrs with a Nikon C1 s+ confocal microscope on a Nikon Eclipse Ti-0E inverted microscope base, as described in previously published methods[134]. The plate was incubated using a plate cover during this time. Images were exported to a lossless multipage TIF from Nikon NIS-Elements and analyzed via an automated MATLB script. This script, as described previously[134], analyzed the images to identify cells, nanoparticles, and Gal8 puncta by

quantification of the fluorescent intensity of each pixel. The Gal8 signal intensity was normalized to the relative cell count, which was quantified by intensity of GFP signal, to determine relative endosomal escape. Relative NP uptake was determined by normalizing the Cy5 signal inside the cell by the Cy5 signal outside the cell. Data points display the mean and error bars display the standard error of the mean.

Black Hole Quencher Assay

The nanoparticle library and 5k PEG-DB and 20k PEG-DB Ppxs were prepared loaded with equal amounts of TAMRA siRNA and BHQ2 siRNA. These nanoparticles and Ppxs were plated in a black-walled 96-well plate at a dose of 100nM in either a 50% fetal bovine serum (FBS) solution or a 270 mM sucrose solution. Each well was prepared in triplicate. Fluorescence emission intensity after excitation at 546 nm was measured at 576 nm using a fluorescence plate reader (Tean Infinite F500). The plate was then shaken for five sec in the plate reader and a reading was taken every two min over the course of ~80 min. All the fluorescence measurements for the FBS wells were normalized to the fluorescence intensity in the sucrose wells. A two-way ANOVA with multiple comparisons was done in Graphpad Prism to calculate significance between groups.

Statistical Methods

Unless otherwise stated, all statistical calculations were completed using a one-way ANOVA with Tukey multiple comparisons test in Graphpad Prism. Reported data are all shown as mean and standard error, unless otherwise stated. Significance was determined using $\alpha = 0.05$.

3.3 Results

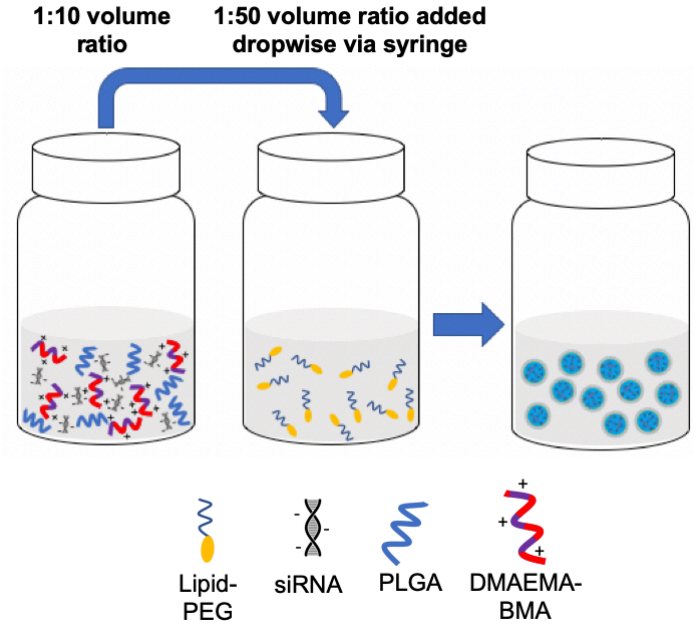

Figure 6. Formulation of nanoparticles via an oil in water (O/W) nanoprecipitation.

Characterization of Nanoparticles

The nanoparticle design consists of three distinct polymer components: a lipid-PEG corona to increase bioactivity, a pH-responsive random copolymer of dimethylaminoethyl methacrylate (DMAEMA) and butyl methacrylate (BMA) (DB) to enhance endosomal escape, and poly(D,L -lactide-co-glycolide) (PLGA) to form a "solid" core and enhance the crystallinity of the NP (**Figure 5**). The endosomolytic pH-responsive polymer was synthesized at either a 50:50 mole% of DMAEMA:BMA (polymer "50B") or a 60:40 mole% of DMAEMA:BMA (polymer "40B") with a degree of polymerization of approximately 150 and molecular weight of ~20 kDa. In all formulations, the amount of siRNA used remained constant and an amine:phosphate ratio (N^+:P^-) of 10 was used. Along with varying the use of 40B and 50B in the NP formulations, the amount of PLGA used was varied such that the final NP would consist of

either 20%, 40%, 60%, or 80% DB by mass. Thus, a library of eight NPs was formulated: 20% 40B, 40% 40B, 60% 40B, 80% 40B, 20% 50B, 40% 50B, 60% 50B, and 80% 50B.

NPs were synthesized using an oil-in-water emulsion (O/W): PLGA, DB, and the siRNA were dissolved in an acetonitrile solution and then added via a syringe to a stirring aqueous solution containing lipid-PEG (**Figure 6**). The average hydrodynamic diameter of all the NPs was similar, ranging from 146 nm to 171 nm, with all having a polydispersity under 0.25. **Figure 7** shows a representative dynamic light scattering (DLS) curve, indicating the size distribution of the 60% 50B NP formulation. Further, the surface charge was similar for NPs of each DB polymer, with all the particles being appreciably cationic: zeta potential for the 40B NPs ranged from 36-41 mV and the 50B NPs ranged from 20-26 mV (**Table 1**).

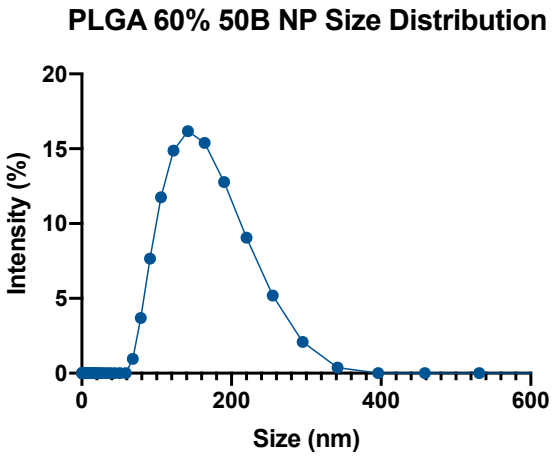

Figure 7. Representative size distribution of the PLGA 60% 50B NPs as measured by DLS.

In order to determine the encapsulation efficiency of the siRNA in the NPs, the O/W suspension of nanoparticles was analyzed via a Ribogreen assay. The encapsulation efficiency was quantified by determining the amount of free siRNA in the emulsion. The entire NP library showed high encapsulation efficiencies of 89%-98% (**Table 1**). As a whole, the characterization

of the NPs indicated that the various formulations did not differ in terms of size, surface charge, or siRNA loading efficiency.

Table 1. NP characterization

Nanoparticle	Avg Size (d.nm)	PDI	Zeta Potential (mV)	Encapsulation Efficiency (%)
20% 40B	151.7	0.237	40.3 ± 6.78	95.81
40% 40B	160.6	0.198	40.0 ± 6.58	97.26
60% 40B	169.7	0.170	36.9 ± 5.29	97.59
80% 40B	170.6	0.210	39.5 ± 6.09	96.92
20% 50B	151.7	0.180	25.7 ± 5.80	89.76
40% 50B	145.9	0.198	22.6 ± 5.12	92.85
60% 50B	146.0	0.193	20.9 ± 4.00	92.99
80% 50B	150.0	0.202	23.8 ± 4.99	91.84

In Vitro Toxicity

To elucidate differences between the NP formulations, we screened the library for differences in cytotoxicity. MDA-MB-231 breast cancer cells were incubated with NP treatments at doses of 100 and 50 nM siRNA for 24 hrs. After this incubation, the cells were returned to fresh media for another 24 hrs. Cell viability was then quantified (48 hrs after initial treatment) using the CellTiter-Glo luminescent assay (**Figure 8**). The 40B NPs generally demonstrated higher levels of cell death than the 50B formulations across all treatments, except for the 100 nM treatment with 20% DB. Further, within a single DB polymer, a clear trend was observed where higher percent DB increased toxicity in both 100 and 50 nM doses. Additionally, the cell viability was above 80% for 50 nM treatments of the 20%, 40%, and 60% 50B NPs 48 hrs post

treatment. This suggests that the 40B formulations are overall more toxic than their 50B counterparts, and increasing percent DB content leads to greater cytotoxicity.

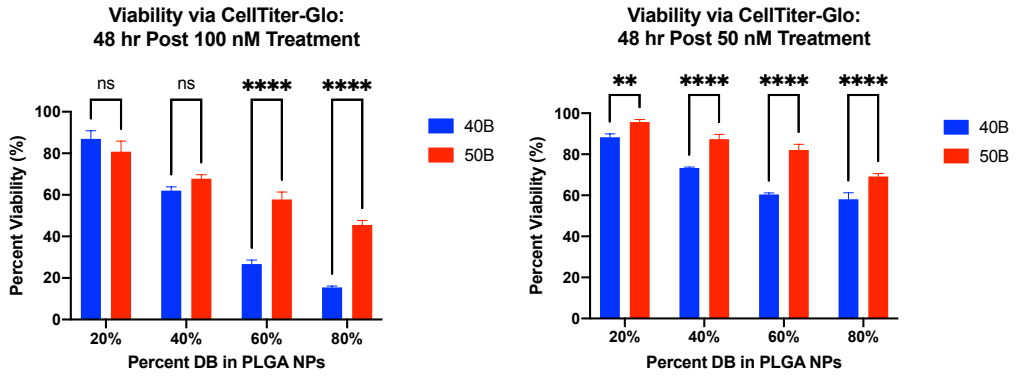

Figure 8. MDA-MB-231 breast cancer cell viability 48 hr post treatment with the NP library at (**A**) 100 nM and (**B**) 50 nM doses of siRNA (**p < 0.01, ****p < 0.0001).

In Vitro Luciferase Silencing

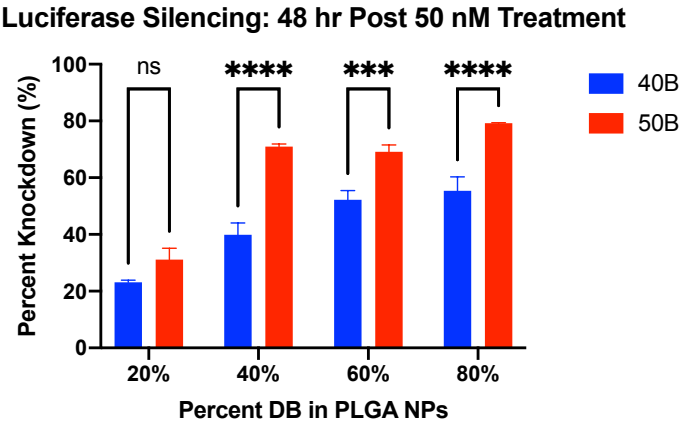

Figure 9. Silencing of the model gene luciferase in Luc-MDA-MB-231 breast cancer cells 48 hr post treatment with 50 nM siRNA doses of the NP library (***p < 0.001, ****p < 0.0001).

Knockdown of the model gene luciferase in luciferase-expressing MDA-MB-231 (Luc-MDA-MB-231) was evaluated to identify differences in bioactivity within the NP library (**Figure 9**). Given the high (>50%) toxicity observed with select 100 nM doses, a 50 nM dose of siRNA was used to treat the Luc-MDA-MB-231 cells. The luciferase activity was quantified in a similar manner to the toxicity: readings were taken 48 hrs after initial treatment. The 40B NPs exhibited poorer luciferase silencing than the 50B library. Further, as the DB percentage

increased, the luciferase silencing ability also increased. The 40%, 60%, and 80% 50B 50 nM treatments were able to knock down >70% luciferase activity in the cells. Therefore, there is an inverse relationship between toxicity and activity of NP library, and the 50B NPs outperform the 40B formulations.

In Vitro Endosomal Escape

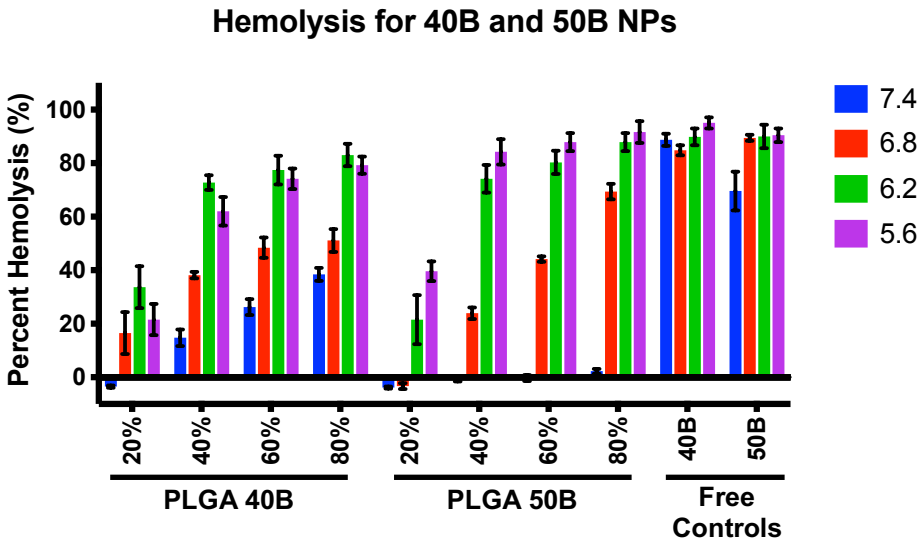

Figure 10. Hemolysis assay with the NP library and free DB polymer controls. RBCs were treated with 40 ug/mL of polymer.

In order to test the endosomal escape ability of this NP system, a hemolysis assay was conducted with the NP library. This assay measures the ability of the NPs to disrupt red blood cell (RBC) membranes in a pH-responsive manner. NPs were incubated in buffered solutions corresponding to the lysosome, late/early endosome, and extracellular space (pH 5.6-7.4). The membrane disruptive ability was then quantified by the amount of hemoglobin released (**Figure 10**). Free 40B and 50B were used as controls, and 40 ug/mL doses of the polymer resulted in lysis of RBCs at all pH values. However, there was still a trend of increasing membrane disruption with decreasing pH. The 40B formulations, particularly the 40%-80%, showed activation at physiologic pH (7.4). On the other hand, the 50B formulations generally showed activation at a pH of 6.8, consistent with the pH of the early endosome[133]. Overall, the NP

formulations show a clear trend that as pH decreases, membrane disruption increases: the pH responsive function of DB. Further, as DB percentage increases, membrane disruption increases. Given the high cytotoxicity, poor activity, and extracellular pH activation of membrane disruption of the 40B NP library relative to the 50B NPs, the 40B NPs were not studied further.

Visualization of NP Uptake and Endosomal Escape

To further understand how 50B NP library interacts with cells, we conducted a Gal8 intracellular tracking assay. As described previously, this assay allows for visualization of endosomal escape in cells in real time and can be combined with the use of fluorescently labeled drugs to visualize cell uptake[134].

In order to visualize cellular uptake of NPs via fluorescent microscopy, the NP library was formulated with siRNA conjugated to the fluorescent dye Cy5 (**Figure 11A**). Images were obtained over a period of 10 hrs for cells treated with both 50 nM and 12.5 nM doses of the NP library and the relative intracellular fluorescence intensity was quantified via a MATLAB script (**Figure 11B,C**). This data demonstrates that the entire 50B NP library is internalized rapidly by cells. Cellular uptake of 40-80% 50B NPs was similar, while it trended downward for 20% 50B NPs at the 12.5 nM dose.

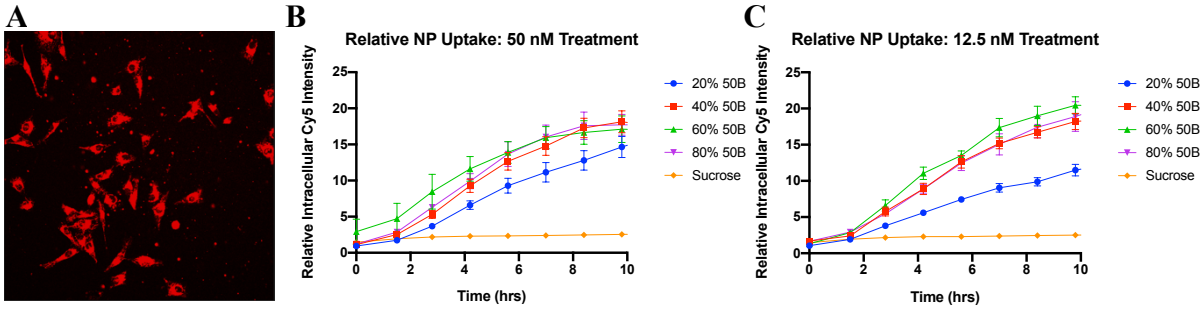

Figure 11. (**A**) Representative image of NP cell uptake after 10 hr of incubation with a 50 nM treatment of Cy5 labeled siRNA loaded 60% 50B NPs. Quantification of relative intracellular fluorescent signal over a 10 hr time course to quantify cellular uptake with (**B**) 50 nM and (**C**) 12.5 nM Cy5 labeled siRNA loaded NP treatments.

Endosomal escape is visible in real-time via the Gal8 assay as fluorescent puncta (**Figure 12A**). The Gal8 intensity relative to the fluorescent intensity of the cells was calculated for the 50 nM dose of the 50B NP library over a period of 10 hrs (**Figure 12B**). Relative Gal8 intensity increased with time for all the 50B formulations, consistent with the increase in NP uptake by the cells as time progresses. Of the four treatments, the 20% 50B NPs exhibited the lowest Gal8 activity. Further, there was no clear difference in endosomal escape between the 40%-80% 50B NPs. Overall, the 40-80% 50B NPs exhibited a potent ability to disrupt the endosomal membrane, providing further support for their use as a siRNA delivery vehicle.

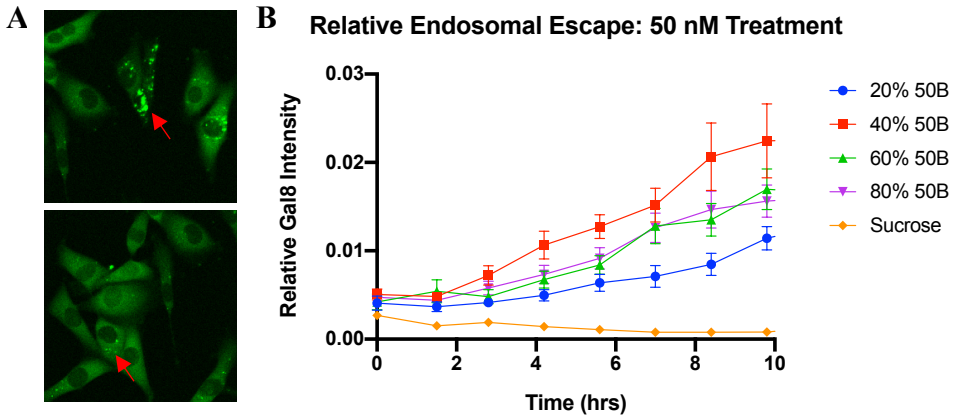

Figure 12. (**A**) Representative images of 60% 50B NP endosomal escape via the Gal8 Assay. Green puncta indicate endosomal disruption. (**B**) Quantification of relative Gal8 signal over a 10 hr time course to quantify endosomal escape.

Stability of Nanoparticles

In order to quantify the stability of the 50B NPs, a Black Hole Quencher assay was used. NPs were loaded with a siRNA solution of 50% siRNA labeled with the fluorophore TAMRA and 50% siRNA labeled with BHQ2. In this assay, the fluorescent signal increases as the particles degrade. Our lab previously designed siRNA loaded Ppxs consisting of 5 or 20 kDa PEG conjugated to DB[12]. These 5k and 20k PEG Ppxs were used as controls to elucidate the impact the addition of PLGA has on stability of the NP design. NPs and Ppxs were incubated in 50% fetal bovine serum (FBS) or 270mM sucrose solutions and the fluorescence was measured

regularly over a period of 80 minutes. The fluorescence intensity of the particles in serum was normalized to the fluorescence intensity in sucrose (**Figure 13**). The entire 50B NP library outperformed both Ppxs. Further, the 50B NP library proved to be very stable, with the highest fold change in fluorescence under 1.2. Overall, this data shows that the inclusion of PLGA in the 50B NP library is significantly improves stability compared to the previously published 5k or 20k PEG-DB Ppxs.

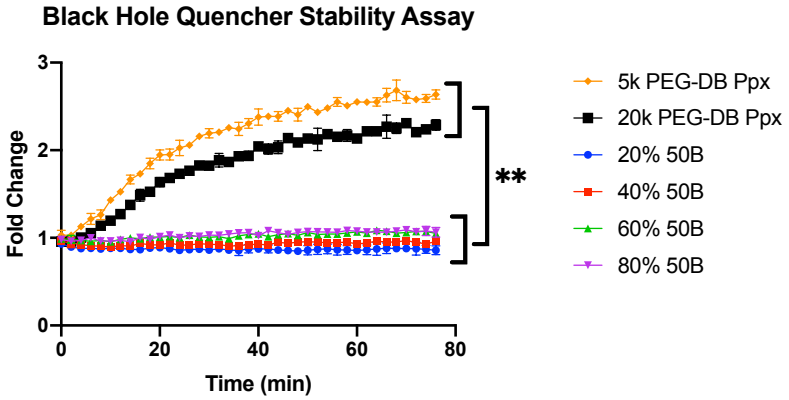

Figure 13. Quantification of the Black Hole Quencher assay to indicate relative release of siRNA from NPs when incubated in 50% FBS relative to a sucrose solution (**p < 0.01).

In Vitro Dose Response to 50B NPs

In order to investigate the potency of the 50B formulations, we repeated the luciferase silencing and cell viability studies with Luc-MDA-MB-231 breast cancer cells with 50 nM, 25 nM, 12.5 nM, and 6.25 nM siRNA treatments of the 50B NP library. Luciferase signal was quantified 48 hrs after treatment and showed similar trends compared to the 100 nM and 50 nM treatments (**Figure 14A**). As the concentration of the NP treatment decreased, luciferase silencing decreased linearly for all of the groups except for the 20% 50B NPs, for which activity was similar. For the 40-80% 50B NPs, we observed ~45% luciferase silencing even at the lowest dose, indicating high potency of these formulations. The overall trend remained the same as

before: as percent DB increased, the gene knockdown ability increased. Further, the degree of luciferase silencing across the 40%-80% 50B NPs was very similar.

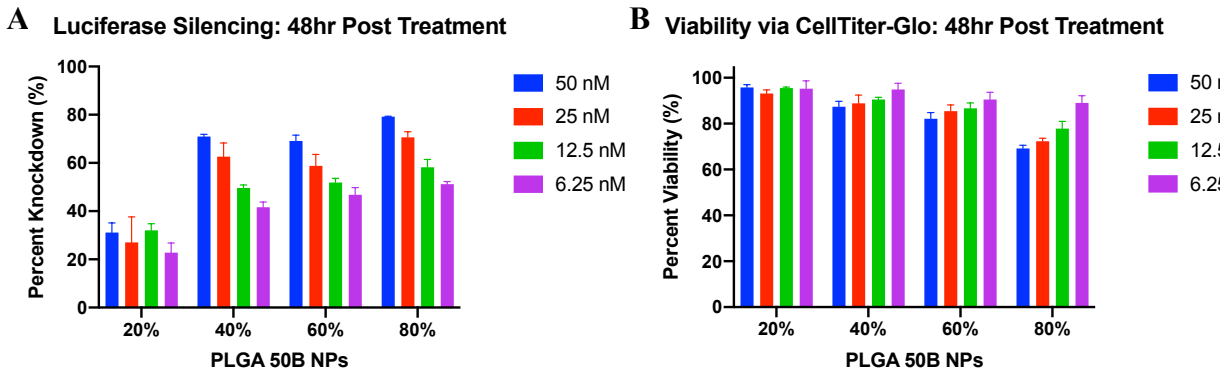

Figure 14. Dose responsive curve of (**A**) luciferase silencing and (**B**) cell viability in Luc-MDA-MB-231 breast cancer cells 48 hr post treatment with the 50B NP library.

Cell viability was quantified via a CellTiter-Glo assay 48 hrs after treatment, as done previously (**Figure 14B**). Again, the results and trends were very similar to those observed in the 100 nM and 50 nM treatments. As the percent DB within the NPs increased, the cell viability decreased. The extent of toxicity decreased as the dose of NPs decreased for all NPs other than the 20% 50B NPs, for which cell viability remained around 90%. At lower doses, the 40%-80% 50B NPs also have low toxicity, with cell viability >80%.

3.4 Discussion

The delivery of siRNA poses a major challenge for its use as a therapeutic agent. siRNA is an extremely potent regulator of gene expression, but its potential cannot be realized without overcoming delivery challenges[3]. For this reason, there is great need for a delivery system that is stable *in vivo*, able to deliver siRNA to the cell cytosol, and is biocompatible. Limitations with regards to these factors have clear impacts on the efficacy of the system.

Our lab has previously published on a variety of Ppx designs of PEG-DB for the delivery of siRNA[11,12,132]. While these NPs were pH responsive and able to actively escape the endosome, they had limitations with regards to stability. For this reason, we proposed and validated a solid

NP carrier of siRNA made up of DMAEMA-co-BMA and PLGA with a lipid-PEG corona. To optimize this NP formulation, we focused on varying the polymers comprising the NP core. Specifically, we varied the ratio of DMAEMA to BMA in the DB copolymer and the ratio of DB to PLGA in the NP.

In order to identify how the polymer composition of the NP impacted its physical characteristics, we tested size, surface charge, and encapsulation efficiency. The particles were generally around 150 nm with a polydispersity under 0.2. The surface charge was cationic and around 22 mV for the 50B NPs and around 40 mV for the 40B NPs. Encapsulation efficiency of siRNA for all these particles was ~ 90%. Overall, this analysis suggests that varying the DB content does not cause significant difference in the characteristics of the particles. Thus, while it is known that differences in size and surface chemistry can affect pharmacokinetics[135], these physical properties should not contribute to the differences that arose internally within the 50B and 40B NP formulations during *in vitro* testing. Rather, these differences can be attributed to the chemical composition of the NP system. However, the difference in cationic surface charge between the 50B and 40B NP library is worth noting.

Next, we tested *in vitro* cytocompatibility and silencing of the NPs. Cell viability 48 hrs post treatment with the NPs showed that the 40B NPs generally appeared to be significantly more toxic compared to their 50B counterparts, indicating the possible toxicity of the 40B system. This is consistent with previous experiments in our lab showing the 40B polymer has higher toxicity than the 50B polymer when incorporated in porous silicon NPs[136]. Additionally, this increased toxicity for the 40B NPs may be explained by the higher cationic surface charge of these particles[137]. The experiment also showed a clear trend across the NPs of the toxicity increasing as DB content in the NP formulations increased. This supports our hypothesis that

PLGA provides stabilization and shields the effects of the DB component. This was followed by an experiment testing the Luc silencing levels of the NP library in Luc-MDA-MB-231 cells 48 hrs after treatment. Here, a trend of increasing silencing with increasing DB content was observed. This data also indicated that the 40B NPs generally performed worse in terms of gene knockdown compared to the 50B NPs. An optimal formulation would balance toxicity with activity, ensuring optimization of bioactivity and biocompatibility. Based on these initial assays, the 50B 40% and 60% formulations were promising.

We wanted to better understand the source of differences in toxicity and activity across the library, particularly because the similarity in physical characteristics suggests that these differences are caused by the polymer components. From the activity and cytotoxicity data, it is clear that the DB content impacts the behavior of the particle. DB was included in this system to facilitate endosomal escape via a pH-responsive mechanism, as has been previously shown[11]. However, DB can also cause inherent toxicity and is a reason why previous approaches utilized PEGylation[11], and we utilized PLGA and a lipid-PEG corona. Therefore, to understand the impact of DB in the system we conducted a hemolysis assay, which models membrane disruptive capabilities as a function of the pH observed in endo/lysosomal trafficking. This data showed the pH responsive nature of DB across the NP formulations: as the pH decreased from the extracellular pH of 7.4 to the lysosomal pH of 5.6, the membrane disruptive ability of the NPs increased. However, the 40B 40%-80% particles show membrane disruptive activation at the extracellular pH of 7.4. This is consistent with data from previous experiments showing 40B-containing NPs have a membrane disruptive behavior at extracellular pH values[136]. This indicates that these 40B formulations are most likely rupturing the cells during treatment, leading to higher toxicity. The same is not observed for the 50B particles, providing a reason for lower

toxicity in the MDA-MB-231 cells. Further, this offers a possible explanation for why the 40B NPs underperform the 50B NPs in terms of Luc silencing. The inherent toxicity of the 40B polymer may lead to reduced transfection of the siRNA. There is also a clear trend that as DB percent increases the extent of membrane disruption at all the pH conditions tested increases. This provides evidence for why higher activity is observed in the higher content DB particles; they are better suited for endosomal disruption and delivery of the siRNA payload. This also supports the fact that toxicity increases with increasing DB content. PLGA appears to shield the DB polymer and reduce its membrane disruptive ability.

Based on this analysis of the entire NP library, it was clear that the 40B NPs were more toxic and less active than their 50B counterparts, most likely due to their stronger membrane disruptive activity. For this reason, we eliminated the 40B NPs and only moved forward with testing the 50B NP library. To further understand cell response to the 50B NPs, we conducted an uptake and Gal8 study over a period of 10 hrs. NPs were loaded with Cy5 labeled siRNA and used to treat Gal8-MDA-MB-231 cells at 50 nM and 12.5 nM doses. This allowed for real time visualization of both NP uptake and endosomal escape. While all formulations exhibited increasing cell uptake as a function of time, the 20% 50B NPs had the lowest uptake out of the four groups. A similar trend was observed regarding endosomal escape via the Gal8 assay. These results indicate that the reduced activity exhibited by the 20% 50B NPs could be partially explained by reduced cell uptake. On the other hand, the 40%-80% 50B NPs had very similar responses, suggesting strong endosomal escape abilities. However, there was no clear difference or trend between the 40%-80% groups in terms of cell uptake or endosomal escape. Overall, this is encouraging for *in vivo* applications of this siRNA delivery system since the Gal8 assay has

been shown to be a better predictor of bioactivity than Lysotracker colocalization, pH-dependent hemolysis, or cellular uptake[134].

An important reason for incorporating PLGA into the design of these NPs was to increase the stability of the particles. Previously studied PEG-DB Ppxs faced issues with stability when posed with a physiologically relevant stability challenge, with over 40% of the loaded dose being released under 80 minutes[12]. Therefore, we conducted a Black Hole Quencher assay to quantify the stability of the 50B NP library and compare it to these previously studied 5K-PEG- and 20K-PEG-DB Ppxs. This assay showed that the 50B NPs were significantly more stable than the Ppxs over a period of 80 minutes in a 50% FBS challenge. This supports that PLGA increased the stability of the NPs. However, no clear differences were observed among the 50B NP formulations.

To better understand the potency of the formulations, we repeated the luciferase knockdown and CellTiterGlo viability assay with varying doses of the 50B NPs (doses ranged from 50 nM to 6.25 nM). While decreasing the dose generally led to a decrease in activity and toxicity for the 50B NPs, the overall trends remained the same. The 20% 50B NPs had lower toxicity and activity while the 80% 50B NPs had higher toxicity and activity compared to the rest of the groups. However, again no clear differences were observed between the 40% and 60% 50B NPs. The >40% gene knockdown at doses as low as 6.25 nM was very encouraging with regards to the efficacy of these treatments and an improvement over previously published siRNA delivery systems[12].

As a whole, this data set suggests that this novel NP formulation is extremely potent and able to deliver its siRNA load to the cell cytosol via endosomal escape. Further, it is clear that the PLGA provides a stabilizing and shielding effect for the DB component. Characterization of

these NPs suggests that the two lead candidates are the 40% and 60% 50B NPs. However, no clear differences were observed between these two formulations. Given the similarity of these two NPs, it does not appear that the PLGA to DB ratio in this range makes an impact on particle properties. We proceeded to test the 60% 50B NP as the lead candidate in vivo.

3.5 Conclusion

A stable, endosomolytic, and biocompatible delivery vehicle for siRNA is essential for its translation as a therapeutic drug. Here, we proposed and optimized the design of a NP system composed of a hybrid core of PLGA and DMAEMA-co-BMA with a lipid-PEG corona. This design was intended to increase stability, deliver siRNA to the cytosol, and avoid toxicity. In order to determine the optimal formulation that met these goals, we varied the type of DB copolymer used and the ratio of DB to PLGA in the core of the NP. A library of eight NPs was tested for their ability to be taken up by cells, their activity, their cytotoxicity, their stability when subjected to a serum challenge, and their membrane disruptive ability. These tests led us to the conclusion that 40% 50B and 60% 50B NPs are optimal for the delivery of siRNA. These particles were able to silence gene expression in cells via endosomal escape with low toxicity. Further, they were significantly more stable than previously published NP designs. While the *in vitro* activity of these particles is evident, further testing is required to determine their efficacy *in vivo*.

Chapter 4: *In vivo* Testing of PLGA-DB-siRNA Nanoparticles as a Therapeutic for OA

4.1 Introduction:

OA is a chronic degenerative disease that affects more than 25% of people over the age of 45[103], causing pain and loss of mobility. In addition to reducing quality of life for afflicted patients, this disease poses an immense burden on the US healthcare system, costing over $44 billion annually[103]. Despite the prevalence and cost of this disease, there is still no approved DMOAD on the market. Current pharmaceutical treatment focuses on palliative care[5]. For this reason, there is major incentive and need for the development of DMOADs.

One appealing option to modify the molecular underpinnings of OA is the specific silencing of MMP13[129]. While previous studies showed efficacy with the use of small molecule inhibitors of MMP13 to treat OA, there were issues with nephrotoxicity due to off-target effects[131]. However, IA delivery of siRNA specific for MMP13 offers a promising approach for the treatment of OA by addressing the previous issues of local drug accumulation and off-target effects. The major limitation for the use of siRNA has been its delivery. Our laboratory has previously used IA injected microPlates[7] and type II collagen-targeting NPs[8] for the delivery of MMP13-specific siRNA, allowing for the treatment of OA. Both of these approaches showed the ability to induce MMP13 silencing, retention up to a period of 25 days, and reductions in disease progression marked by reduced cartilage degradation, meniscal deterioration, and other histological markers. Our optimized hybrid PLGA-DB NP offers another approach for the delivery of siRNA to the joint space. Further, the modular design of the NP system has a number of advantages, particularly with the possibility of future surface modification for cell targeting

and retention. In this chapter, we demonstrate proof-of-concept testing of our NP system for the delivery of MMP13 siRNA and treatment of OA.

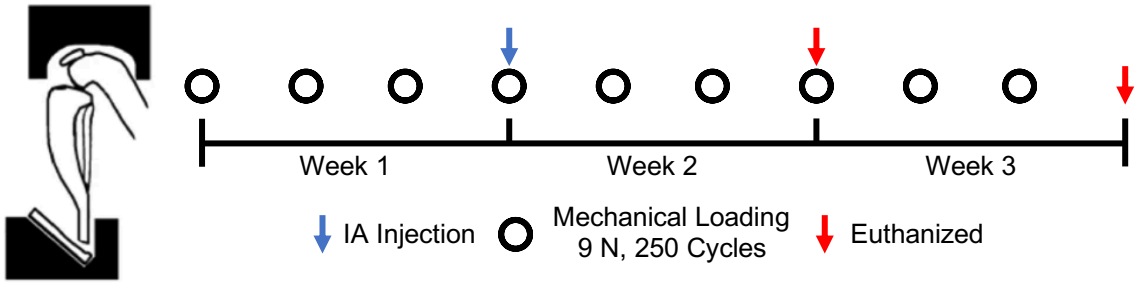

Figure 15. Schematic of the loading and treatment regimen used to study the efficacy of the siRNA loaded 60% 50B NPs.

To test the efficacy of our optimized NP design as an IA delivery system for siRNA, we treated a murine model of OA with a single injection of our MMP13-specific siRNA-loaded PLGA-DB-siRNA NPs (**Figure 15**). To understand IA pharmacokinetics, we tracked siRNA retention over a period of one month. Further, pharmacodynamics was evaluated by measuring MMP13 silencing ability of the siRNA 7- and 14-days following injection of our therapeutic NPs. The ability of this disease modifying system to alleviate pain was also measured as an indication of the functional benefits of this system. The overall goal of these experiments was to test the viability of our optimized NP system for siRNA delivery *in vivo*. Further, the lack of DMOADs makes the treatment of OA an ideal candidate for siRNA-based therapeutics.

4.2 Materials and Methods

Materials

In Vivo Nanoparticle Dose Formulation

NPs for the *in vivo* formulations were prepared using the same methods as for the *in vitro* NPs. To concentrate the solution, the emulsion was centrifuged at 1000xg for 5 min (Centrifuge 5804, Eppendorf) in 15 mL batches. After each spin, the spin filter tube was replenished with

additional emulsion solution, and the centrifugation was repeated. DSPE-PEG was also added between spins to prevent stripping of the PEGylation from the NPs. Once all NPs were collected, the NP suspension was washed with sucrose; 15 mL of 270 mM sucrose was used to resuspend the concentrated NPs and centrifugation was repeated. The concentrated NPs were brought up with 270 mM sucrose to a volume such that 15 uL contained 12 ug of siRNA. This solution was flash frozen and stored at -20°C.

Mechanical Loading of Mice and Nanoparticle Treatment

For the mechanical loading model of PTOA, 32 8-week-old, male, C57 mice were obtained from Charles River Labs. The mice were housed under standard conditions (18-23°C, 40-60% humidity, 12 hr light:12 hr dark cycle) in Vanderbilt University's rodent housing facilities in compliance with all procedures reviewed and approved by the IACUC. All relevant IAVUV animal-use guidelines and ethical regulations were followed in animal work conducted for this study.

C57 mice were subjected to mechanical loading of their knees to model PTOA, as described in previously published methods[8]. Noninvasive repetitive joint loading consisted of subjecting mice anaesthetized with 3% isoflurane to 250 cycles of compressive mechanical loading with a max force of 9 N. This loading cycle was repeated three times per week for the duration of the study.

Following one week of mechanical loading, mice were injected IA with 15 uL 0.4 mg/kg siRNA doses of 60% 50B NPs. 8 mice were injected in the right knee with NPs loaded with Cy5 siRNA, and 6 mice were loaded in both knees with NPs loaded with MMP13 siRNA. 6 mice were untreated controls. Mice were euthanized 7 and 14 days post-injection.

In Vivo NP Retention

Intravital imaging was performed on mice using an IVIS Lumina III imaging system in order to determine the retention of the NPs in the joint space. Mice injected with Cy5-siRNA-NPs were imaged daily. The fluorescence intensity of the knee joint was compared to the intensity of untreated control mice. Data is shown as mean and standard error of the mean.

Design of ACL Rupture Fixtures

Fixtures to induce an ACL rupture in mice were designed in Autodesk Fusion360 and modeled off of existing designs sent by Blaine Christiansen, Ph.D and Tristan Maerz, Ph.D.

RT-PCR of Cartilage Samples

RT-qPCR was done on cartilage samples collected 7 and 14 days post treatment from mice treated with MMP13 NPs. PCR was performed using TaqMan primers (ThermoFisher Scientific) as outlined by the manufacturer. The MMP13 primer used was Mm00439491_m1.

Functional Readout of Mice Pain

The SMALGO algometer (Bioseb, FL, USA) was used as a functional readout of pain sensitivity in mice intravitally throughout the duration of the study. Progressive mechanical pressure was applied to the knee joint while measuring with the pressure-based analgesimeter until a noticeable reaction from the mouse (scream, shudder, paw removal, etc.) occurred. The final applied weight in grams was recorded as the sensitivity of the mouse.

Statistical Methods

All statistical calculations were completed using a one-way ANOVA with Tukey multiple comparisons test or two-tailed Student's t-test in Graphpad Prism. Reported data are all shown as mean and standard error, unless otherwise stated. Significance was determined using $\alpha = 0.05$.

4.3 Results

Retention of Nanoparticles in Murine Knee

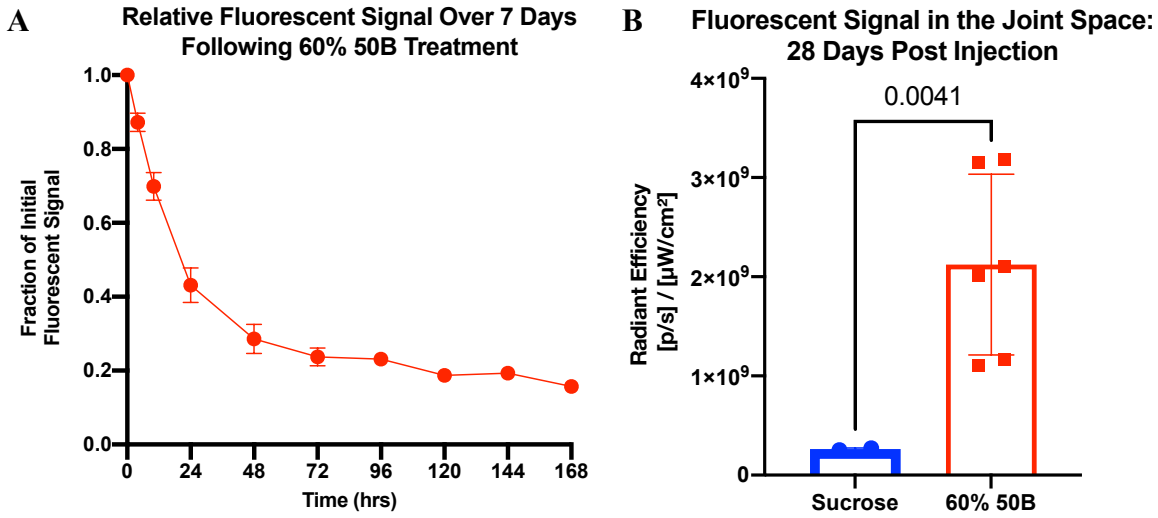

Figure 16. (**A**) Relative intravital fluorescent signal of the fluorescently labeled siRNA following IA treatment with 60% 50B NPs. (**B**) Fluorescent signal of the joint *ex vivo* 28 days after treatment with Cy5-Scr-siRNA 60% 50B NPs.

A murine model of OA was used in this study to test the pharmacodynamics and pharmacokinetics of the MMP13-siRNA loaded 60% 50B NPs. OA was induced in mice via noninvasive repetitive mechanical joint loading. Both the right and left knee of 8-week old C57 mice were subjected to 250 cycles of compressive mechanical loading at 9N three times over the course of a week, followed by IA injection of 0.4 mg/kg doses of either Scr-Cy5 fluorophore-labeled siRNA or MMP13-siRNA loaded NPs, and continued loading 3x per week until euthanasia (**Figure 15**). The use of Cy5 labeled siRNA allowed for intravital IVIS fluorescence imaging of the joint space and subsequent pharmacokinetic analysis. Intravital imaging of the joint showed retention of over 15% of the initial drug dose over a period of seven days (**Figure 16A**). Further, a fluorescent signal was visible even after 28 days when the joint was isolated and skin removed (**Figure 16B**).

In Vivo MMP13 Silencing

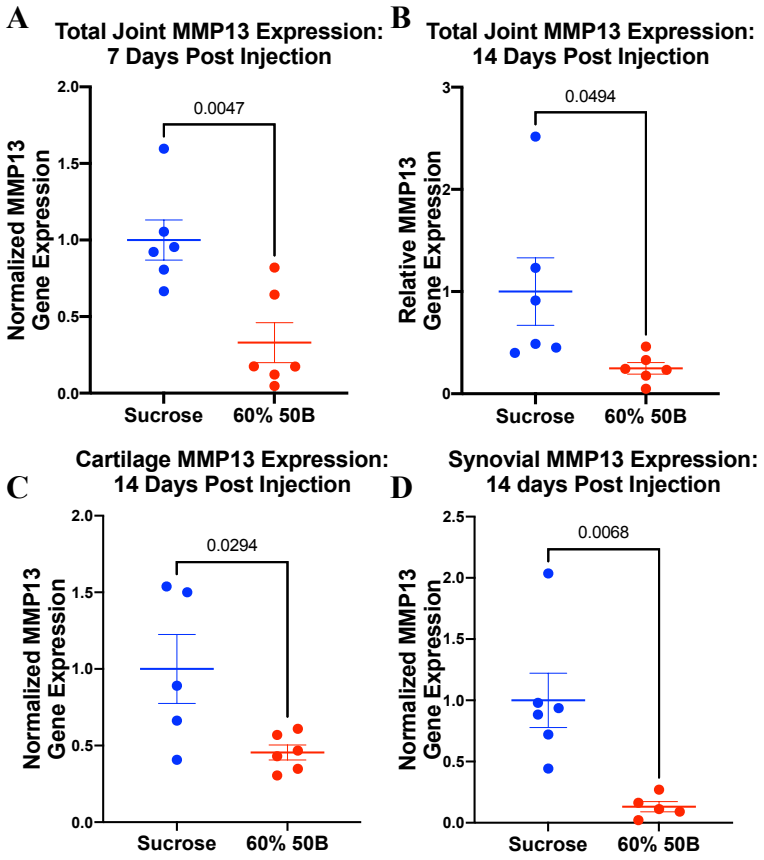

Figure 17. Relative MMP13 gene expression in the joint as a whole (combined synovial and cartilage tissue) (**A**) 7 and (**B**) 14 days post IA injection of either sucrose or MMP13-siRNA loaded 60% 50B NPs in a murine model of OA. Relative MMP13 gene expression was also analyzed in (**C**) cartilage and (**D**) synovial tissue separately 14 days after IA injection in a murine model of OA.

To test the efficacy of the NP formulation, cartilage and synovial tissue was collected from the MMP13-siRNA treated mice following euthanasia either 7- or 14-days post IA injection. MMP13 expression was quantified via RT-qPCR in the combined tissue samples (total joint), showing a significant reduction in MMP13 expression compared to sucrose treated controls at both time points after a single injection (**Figure 17A,B**). As further confirmation, we measured MMP13 expression in the synovium and cartilage separately. As with the combined samples, there was a significant reduction compared to sucrose controls (**Figure 17C,D**).

Overall, the NP formulation was able to deliver siRNA and induce gene silencing that lasted at least 14 days with a single IA treatment.

Functional Pressure-Pain Threshold

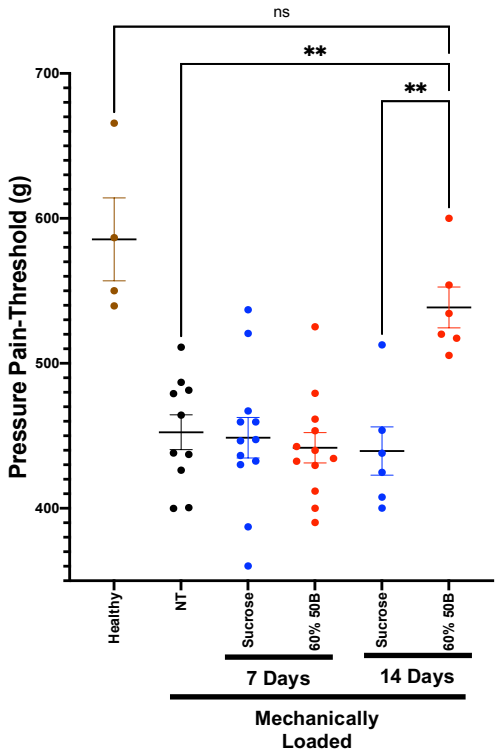

Figure 18. Pressure pain-threshold in healthy or mechanically loaded murine knees following IA treatment with either sucrose or MMP13-siRNA loaded 60% 50B NPs (**p < 0.01).

To determine whether our NP therapeutic had an impact on functional outcomes of the treated mice, we measured the sensitivity of the mice to applied pressure. Using an algometer, we quantified the pressure at which the mice responded, indicating their sensitivity for pain (**Figure 18**). There was no significant difference between the treated and untreated group seven days after injection. However, there was a significant difference in the pain sensitivity of the mice 14 days after treatment with the NP therapeutic compared to those treated with vehicle. Further, at the 14-day time point, there was no significant difference in the pressure-pain threshold between the healthy and the NP treated group. This indicates that a single 0.4 mg/kg

dose of our MMP13 siRNA loaded into 60% 50B NPs was able to lead to a functional change in the pain sensitivity of mice 14 days after treatment, essentially returning to baseline.

4.4 Discussion

OA is a chronic and degenerative disease, causing pain and reducing the quality of life of millions of individuals across the world. However, current pharmaceutical care remains palliative. Many approaches focused on pain relief, like IA injection of corticosteroids, are not suitable for regular use due to associated gastrointestinal and cardiovascular risks[115]. Therefore, there is great need for DMOAD development. While several approaches show promise preclinically, efficacy in clinical trials has been limited. One appealing approach is the specific silencing of MMP13, which has been identified as key proteolytic driver of cartilage loss in OA[6]. Our lab has previously shown disease modification of OA following IA delivery of MMP13-siRNA[7,8]. Here, we proposed the use of our novel NP design as an alternative delivery system for MMP13-siRNA to the joint space.

In order to test the efficacy of the MMP13-siRNA loaded 60% 50B NPs as a novel therapeutic for OA, we treated a murine model of PTOA with 0.4 mg/kg siRNA doses of our NP system. Pharmacokinetic analysis of treated mice indicated retention of over 15% of the initial dose one week following treatment and even retention of siRNA 28 days after a single injection. This NP system shows comparable retention to the microPlate approach previously developed in our laboratory with the Decuzzi group[7]. This is quite impressive, particularly because smaller particles, like these NPs, are usually cleared much more rapidly than therapeutics on the microscale[138,139]. Further, the retention of PLGA-DB NPs compared closely with that of type II collagen targeting antibody conjugated NPs[8]. This extended retention in the joint space is quite remarkable and promising for extended release of the siRNA therapeutic load. This is

particularly impressive given that this system currently has no bioadhesive corona or cell targeting ligand. This lengthy retention is most likely explained by the cationic surface charge, ~+20 mV, of the 60% 50B NPs. These positively charged particles most likely interact with the negatively charged aggrecan layer, increasing retention in the joint space[140,141].

In addition to joint retention, we were interested in quantifying the ability of our NP system to induce gene silencing *in vivo*. Synovial and cartilage tissue from the mice treated with our MMP13-siRNA loaded system following the induction of OA was collected from the joints and MMP13 gene expression was quantified. After seven days, the NP treatment resulted in a significant reduction in the MMP13 expression levels of the combined tissue samples. 14 days after injection, a significant reduction in MMP13 expression in the cartilage sample, the synovial sample, and the combined tissue sample due to the NP treatment was found. This data suggests that a single IA injection of our siRNA loaded NPs was able to attenuate gene expression for at least a period of two weeks. This is comparable to the MMP13 silencing observed with the use of microPlates and shows promise for this innovative NP system to induce gene silencing in vivo[7]. However, longer-term studies are needed in order to determine the full extent of this gene silencing ability, particularly in light of the 4-week retention profile of the NPs. Additionally, histological analysis would be informative to better identify the disease modifying effects of this therapeutic.

Because joint pain is the major symptom that afflicts OA patients, we were interested in the implications of MMP13 silencing on pain response. We quantified the pressure-pain threshold of all mice that were treated with the MMP13 siRNA-loaded NPs. 14 days post injection, mice treated with the NP formulation showed significantly higher pain thresholds. Further, these thresholds were not significantly different from the pain thresholds for untreated

healthy control mice. This suggests that a single IA injection of our NP system was able to reduce pain in the mice, indicating the global, disease-modifying effect of MMP13 knockdown in the joint. This result is particularly striking when considering the damage dealt to the tissue before treatment (1 week of mechanical loading), and suggests that silencing of MMP13 could reverse the effects of established disease, though further investigation is needed to confirm these results. The clinical implication of pain reversal is highly significant, as the majority of patients present with joint pain before intervention is sought[142]. Overall, our data suggests that our NPs are an efficient delivery vehicle for MMP13-siRNA and are highly effective against OA, with lengthy retention in the joint space and both functional and biological improvements in OA pathology.

4.5 Conclusion

OA is a degenerative disease of the joints with no current DMOADs on the market. This disease afflicts millions and has a high cost in terms of both quality of life for the patient and of money for the healthcare system. For this reason, there is a great need for improved therapeutics. In hopes of addressing this need, we proposed the use of our optimized hybrid PLGA and DMAEMA-co-BMA NP with a lipid-PEG corona for the delivery of MMP13-siRNA and the treatment of OA. We tested our novel formulation in a murine model of OA. Pharmacokinetic studies following IA injection of this formulation suggest retention of siRNA in the joint for at least a month. Further, this formulation was able to result in a significant decrease in MMP13 gene expression in the joint space both 7 and 14 days after injection. Not only was the disease modified by this treatment, our NP treatment allowed for recovery to a healthy pressure pain threshold 14 days after treatment. Therefore, not only was our MMP13 siRNA NP able to modulate the OA at a cellular level, it was also able to achieve positive functional outcomes.

While this treatment is extremely promising, longer-term efficacy studies and histological analysis of the joint space following treatment need to be done in order to better understand the success of this therapeutic system.

Chapter 5: Summary and Future Directions

5.1 Synopsis

Over the past 20 years, siRNA has emerged as a potent regulator of gene expression and a promising therapeutic[2]. However, a major limitation with regards to translation is the need for a delivery vehicle. While several nanoparticle designs have been proposed for the delivery of siRNA and some, like patisiran, have even received FDA approval, limitations still exist[91]. In a similar vein, our lab previously published on the design of an endosomolytic Ppx for the delivery of siRNA[11,12,132]. While this approached excelled in its ability to deliver siRNA to the cytosol, it was limited by its stability in circulation. Herein, we proposed an overhaul of our previous design. This system consists of an siRNA loaded nanoparticle made up of three discrete polymer components: PLGA to increase stability of the polymer core, DMAEMA-co-BMA to ensure pH responsive endosomolytic capabilities, and lipid-PEG as the corona to ensure biocompatibility.

In Aim 1, we tested and optimized the proposed NP siRNA delivery system in vitro. In particular, we varied the ratio of DMAEMA to BMA in the DB core polymer and the ratio of PLGA to DB. Testing two different DB polymers and four ratios of PLGA to DB resulted in a library of eight nanoparticles. The physical properties of these particles were characterized, but no major differences were found in size, surface charge, or encapsulation efficiency of siRNA within the 50B and 40B NPs. However, clear trends were observed in terms of cytotoxicity and activity. The 50B formulations were generally significantly less toxic than their 40B counterparts. Further, as the percentage of DB by mass increased in the particles, a clear trend in decreasing cell viability and increasing activity was observed. Further characterization was done to quantify the endosomal escape abilities of the NP library. While all the particles showed clear trends for pH responsive membrane disruption, the 40B particles were found to have a high level

of membrane disruption at extracellular pH. This supports the toxicity results found in in vitro testing. Increasing DB content led to greater membrane disruption, supporting both the activity and toxicity testing of the particles. These results allowed us to down select the 40B NPs and continue testing with the 50B NP cohort. Cell uptake and endosomal escape of the 50B NP library was visualized via fluorescence assays and stability was measured. A similar trend was clear through all this data, the particles as a whole were more stable than historic approaches and the 40% and 60% 50B NPs performed were more active and less toxic. Overall, the studies done in Aim 1 allowed for the optimization of our novel NP design and selection of the 60% 50B NP for further study.

In Aim 2 we tested the ability of the 60% 50B NP to be used as a delivery vehicle for MMP13 to treat OA. OA is an extremely detrimental disease, affecting many individuals. Further, there is no DMOAD available on the market. Treatment primarily focuses on management of pain. MMP13 has been identified as a possible target for OA. So, we tested the efficacy of our NP system when loaded with MMP13. Pharmacokinetic studies after IA delivery indicated that our drug was retained for over 28 days within the joint space. Further, clear reductions in both MMP13 expression in synovial and cartilage tissue seven and 14 days after treatment were observed. Our therapeutic treatment was also able to improve the pain sensitivity of the mice.

Overall, this work shows the development of a stable, endosomolytic, and biocompatible novel NP delivery system of siRNA. This design provides an advancement in the delivery of siRNA by addressing several issues faced by current siRNA delivery modalities, particularly stability and endosomal escape ability. Further, this system shows promise as a therapeutic for OA, a niche where a disease modifying drug has not hit the market.

5.2 Concerns and Limitations

The hybrid PLGA and DB NP proves to be a promising system for the delivery of siRNA. While the modularity of this system allows for easy modification of the surface chemistry, this also makes the system complex. A NP system that consists of three distinct polymer components in addition to a specific siRNA could prove difficult to manufacture at a large scale, posing a limitation for translation. Further, these particles were only tested in one cell line for toxicity and activity. For the use of this system to treat varied diseases, different cell lines will need to be tested. Similarly, *in vivo* studies need be expanded to test for efficacy in different disease models. While this system could be translated for systemic delivery of siRNA, there are concerns that the positive surface charge of the particles may pose toxicity issues in circulation. While this cationic charge likely improved the retention in the joint space because of the anionic aggrecan layer found IA, further studies are needed to understand the impacts this system would have if delivered systemically.

5.3 Future Directions

Given the modular design of this NP system, there are several directions that can be taken to improve its functionality. One option is varying the polymer utilized to stabilize the core of the NP: replacing PLGA. For example, this could consist of using a reactive oxygen species (ROS) scavenging polymer, like poly(propylene sulfide), for the core of the NP. A polymer of this nature would imbue the particle with a ROS-responsive nature and possibly lead to a system that only releases the therapeutic compound under oxidative stress. Another option is varying the biocompatible corona. Lipid-PEG was chosen for the design of this system to increase the stealth of the NP and limit a possible immune response. However, binding or targeting domains within the corona could be used to increase retention of the particles locally or directly target them to

certain cells. Using a bioadhesive corona could be ideal to further increase the retention of these particles within the joint space. Other examples include tumor specific ligands, which could prove useful for these particles as a systemically delivered cancer treatment. This modular design allows for a variety of future studies, all of which would consist of *in vitro* validation followed by *in vivo* efficacy analysis.

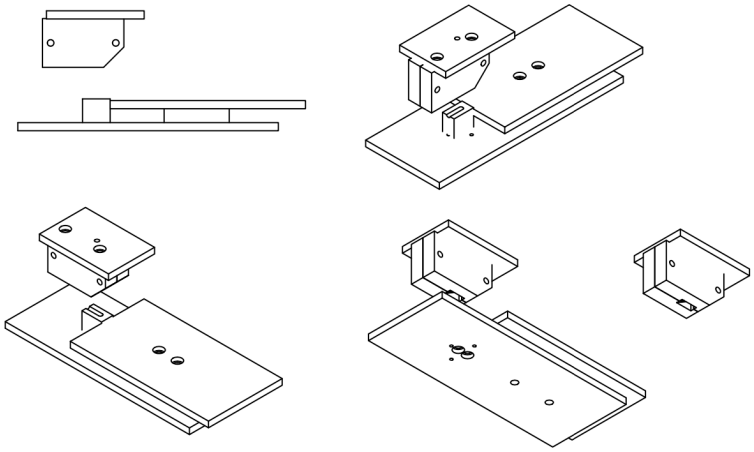

Figure 19. CAD of platforms that will be used to induce OA in mice by rupturing the ACL via a single force causing tibial compression overload.

With regards to the use of the 50B 60% NPs for the delivery of MMP13 siRNA for the treatment of OA, further *in vivo* studies are needed to understand the benefits this therapeutic poses. Longer studies that investigate the ability of the system to reduce pain and silence MMP13 are necessary. Histological analysis to determine how this treatment impacts the joint space is also needed. This could give a clearer indication of the local immune response, where the NPs are being retained, and how the cartilage and overall structure of the joint space is impacted by this therapeutic agent. Further studies in different models of OA could also provide more information about the efficacy of the 50B 60% NP system. For this reason, we are currently looking towards testing this formulation in a murine model of OA induced by ACL rupture via a tibial compression overload. CAD files have been made based on resources shared by Professor Tristan Maerz's lab for the establishment of this murine model in our lab (**Figure 19**). In the

coming months, we plan to test the MMP13 siRNA loaded NPs in this model over a course of three and six weeks to better understand the efficacy of our system

5.4 Broader Impacts

This novel NP platforms was shown to be an ideal carrier for siRNA. Given the limitations of existing siRNA delivery solutions, this formulation or a formulation of its type could prove to aid in the translation of siRNA to the clinic. This alone could have major impacts and allow for a generation of novel therapeutics for diseases that have been difficult to treat. One example is OA. Given our in vivo analysis, it appears that our system performs well for the delivery of siRNA IA. Further, it also reduces gene expression and provides positive functional outcomes. There is no current drug on the market that can accomplish these goals for OA. This data is extremely promising for the translation of drugs like this into the clinic. Not only is OA a debilitating disease affecting millions, but it is also poses a heavy economic burden. The possibility of translating this NP formulation for the delivery of siRNA to treat OA could revolutionize how we currently approach treatment of this disease while helping millions.

Chapter 6: Conclusion

There is a great need for siRNA delivery vehicles that are stable, endosomolytic, and biocompatible. Here we proposed the design of a novel hybrid PLGA and endosomolytic DMAEMA-co-BMA NP with a lipid-PEG corona for the delivery of siRNA. This modular NP design was tuned to optimize cytotoxicity and activity of the siRNA load. Further, the optimized NP, a 60% 50B NP, loaded with MMP13-siRNA was tested as a therapeutic for OA. This promising in vivo data and in vitro characterization provides support for this modular polymer NP system as a delivery vehicle for siRNA and the possible treatment of OA.

References

1. Guo, P. *et al.* Engineering RNA for targeted siRNA delivery and medical application. *Adv Drug Deliv Rev* **62**, 650–666 (2010).
2. Zhang, M. M., Bahal, R., Rasmussen, T. P., Manautou, J. E. & Zhong, X. The growth of siRNA-based therapeutics: Updated clinical studies. *Biochemical Pharmacology* **189**, 114432 (2021).
3. Kanasty, R., Dorkin, J. R., Vegas, A. & Anderson, D. Delivery materials for siRNA therapeutics. *Nature Mater* **12**, 967–977 (2013).
4. Ondrésik, M. *et al.* Management of knee osteoarthritis. Current status and future trends. *Biotechnol Bioeng* **114**, 717–739 (2017).
5. DeJulius, C. R., Gulati, S., Hasty, K. A., Crofford, L. J. & Duvall, C. L. Recent Advances in Clinical Translation of Intra-Articular Osteoarthritis Drug Delivery Systems. *Advanced Therapeutics* **4**, 2000088 (2021).
6. Wang, M. *et al.* MMP13 is a critical target gene during the progression of osteoarthritis. *Arthritis Research & Therapy* **15**, R5 (2013).
7. Bedingfield, S. K. *et al.* Top-Down Fabricated microPlates for Prolonged, Intra-articular Matrix Metalloproteinase 13 siRNA Nanocarrier Delivery to Reduce Post-traumatic Osteoarthritis. *ACS Nano* **15**, 14475–14491 (2021).
8. Bedingfield, S. K. *et al.* Amelioration of post-traumatic osteoarthritis via nanoparticle depots delivering small interfering RNA to damaged cartilage. *Nat Biomed Eng* **5**, 1069–1083 (2021).
9. Gavrilov, K. & Saltzman, W. M. Therapeutic siRNA: Principles, Challenges, and Strategies. *Yale J Biol Med* **85**, 187–200 (2012).

10. Convertine, A. J., Benoit, D. S. W., Duvall, C. L., Hoffman, A. S. & Stayton, P. S. Development of a novel endosomolytic diblock copolymer for siRNA delivery. *J Control Release* **133**, 221–229 (2009).
11. Nelson, C. E. *et al.* Balancing Cationic and Hydrophobic Content of PEGylated siRNA Polyplexes Enhances Endosome Escape, Stability, Blood Circulation Time, and Bioactivity in Vivo. *ACS Nano* **7**, 8870–8880 (2013).
12. Jackson, M. A. *et al.* Zwitterionic Nanocarrier Surface Chemistry Improves siRNA Tumor Delivery and Silencing Activity Relative to Polyethylene Glycol. *ACS Nano* **11**, 5680–5696 (2017).
13. Fire, A. *et al.* Potent and specific genetic interference by double-stranded RNA in Caenorhabditis elegans. *Nature* **391**, 806–811 (1998).
14. Elbashir, S. M. *et al.* Duplexes of 21-nucleotide RNAs mediate RNA interference in cultured mammalian cells. *Nature* **411**, 494–498 (2001).
15. Caplen, N. J., Parrish, S., Imani, F., Fire, A. & Morgan, R. A. Specific inhibition of gene expression by small double-stranded RNAs in invertebrate and vertebrate systems. *Proc Natl Acad Sci U S A* **98**, 9742–9747 (2001).
16. Hopkins, A. L. & Groom, C. R. The druggable genome. *Nat Rev Drug Discov* **1**, 727–730 (2002).
17. Wu, S. Y., Lopez-Berestein, G., Calin, G. A. & Sood, A. K. RNAi therapies: drugging the undruggable. *Sci Transl Med* **6**, 240ps7 (2014).
18. Finan, C. *et al.* The druggable genome and support for target identification and validation in drug development. *Sci Transl Med* **9**, eaag1166 (2017).

19. Morrissey, D. V. *et al.* Potent and persistent in vivo anti-HBV activity of chemically modified siRNAs. *Nat Biotechnol* **23**, 1002–1007 (2005).

20. Okumura, A., Pitha, P. M. & Harty, R. N. ISG15 inhibits Ebola VP40 VLP budding in an L-domain-dependent manner by blocking Nedd4 ligase activity. *Proc Natl Acad Sci U S A* **105**, 3974–3979 (2008).

21. Kristen, A. V. *et al.* Patisiran, an RNAi therapeutic for the treatment of hereditary transthyretin-mediated amyloidosis. *Neurodegenerative Disease Management* **9**, 5–23 (2019).

22. Ferrari, M., Sun, T. & Shen, H. Nanovector Delivery of siRNA for Cancer Therapy. *Cancer Gene Ther* **19**, 10.1038/cgt.2012.22 (2012).

23. Davis, M. E. *et al.* Evidence of RNAi in humans from systemically administered siRNA via targeted nanoparticles. *Nature* **464**, 1067–1070 (2010).

24. Kleinman, M. E. *et al.* Sequence- and target-independent angiogenesis suppression by siRNA via TLR3. *Nature* **452**, 591–597 (2008).

25. DeVincenzo, J. *et al.* A randomized, double-blind, placebo-controlled study of an RNAi-based therapy directed against respiratory syncytial virus. *Proc Natl Acad Sci U S A* **107**, 8800–8805 (2010).

26. Haussecker, D. The Business of RNAi Therapeutics in 2012. *Mol Ther Nucleic Acids* **1**, e8 (2012).

27. Setten, R. L., Rossi, J. J. & Han, S. The current state and future directions of RNAi-based therapeutics. *Nat Rev Drug Discov* **18**, 421–446 (2019).

28. Hoy, S. M. Patisiran: First Global Approval. *Drugs* **78**, 1625–1631 (2018).

29. Jinek, M. & Doudna, J. A. A three-dimensional view of the molecular machinery of RNA interference. *Nature* **457**, 405–412 (2009).

30. Elbashir, S. M., Lendeckel, W. & Tuschl, T. RNA interference is mediated by 21- and 22-nucleotide RNAs. *Genes Dev* **15**, 188–200 (2001).

31. Bernstein, E., Caudy, A. A., Hammond, S. M. & Hannon, G. J. Role for a bidentate ribonuclease in the initiation step of RNA interference. *Nature* **409**, 363–366 (2001).

32. Nykänen, A., Haley, B. & Zamore, P. D. ATP requirements and small interfering RNA structure in the RNA interference pathway. *Cell* **107**, 309–321 (2001).

33. Elbashir, S. M., Martinez, J., Patkaniowska, A., Lendeckel, W. & Tuschl, T. Functional anatomy of siRNAs for mediating efficient RNAi in Drosophila melanogaster embryo lysate. *EMBO J* **20**, 6877–6888 (2001).

34. MacRae, I. J., Ma, E., Zhou, M., Robinson, C. V. & Doudna, J. A. In vitro reconstitution of the human RISC-loading complex. *Proc Natl Acad Sci U S A* **105**, 512–517 (2008).

35. Liu, J. *et al.* Argonaute2 is the catalytic engine of mammalian RNAi. *Science* **305**, 1437–1441 (2004).

36. Hutvagner, G. & Simard, M. J. Argonaute proteins: key players in RNA silencing. *Nat Rev Mol Cell Biol* **9**, 22–32 (2008).

37. Zamore, P. D., Tuschl, T., Sharp, P. A. & Bartel, D. P. RNAi: double-stranded RNA directs the ATP-dependent cleavage of mRNA at 21 to 23 nucleotide intervals. *Cell* **101**, 25–33 (2000).

38. Scott, L. J. Givosiran: First Approval. *Drugs* **80**, 335–339 (2020).

39. Scott, L. J. & Keam, S. J. Lumasiran: First Approval. *Drugs* **81**, 277–282 (2021).

40. Dyrbuś, K., Gąsior, M., Penson, P., Ray, K. K. & Banach, M. Inclisiran—New hope in the management of lipid disorders? *Journal of Clinical Lipidology* **14**, 16–27 (2020).
41. Machin, N. & Ragni, M. V. An investigational RNAi therapeutic targeting antithrombin for the treatment of hemophilia A and B. *J Blood Med* **9**, 135–140 (2018).
42. Second RNAi drug approved. *Nature Biotechnology* **38**, 385–385 (2020).
43. Dowdy, S. F. Overcoming cellular barriers for RNA therapeutics. *Nat Biotechnol* **35**, 222–229 (2017).
44. Kanasty, R. L., Whitehead, K. A., Vegas, A. J. & Anderson, D. G. Action and reaction: the biological response to siRNA and its delivery vehicles. *Mol Ther* **20**, 513–524 (2012).
45. Blanco, E., Shen, H. & Ferrari, M. Principles of nanoparticle design for overcoming biological barriers to drug delivery. *Nat Biotechnol* **33**, 941–951 (2015).
46. Jarad, G. & Miner, J. H. Update on the glomerular filtration barrier. *Curr Opin Nephrol Hypertens* **18**, 226–232 (2009).
47. Gao, S. *et al.* The effect of chemical modification and nanoparticle formulation on stability and biodistribution of siRNA in mice. *Mol Ther* **17**, 1225–1233 (2009).
48. Bartlett, D. W. & Davis, M. E. Effect of siRNA nuclease stability on the in vitro and in vivo kinetics of siRNA-mediated gene silencing. *Biotechnol Bioeng* **97**, 909–921 (2007).
49. Sun, Y. *et al.* Enhancing the Therapeutic Delivery of Oligonucleotides by Chemical Modification and Nanoparticle Encapsulation. *Molecules* **22**, E1724 (2017).
50. Ozcan, G., Ozpolat, B., Coleman, R. L., Sood, A. K. & Lopez-Berestein, G. Preclinical and clinical development of siRNA-based therapeutics. *Adv Drug Deliv Rev* **87**, 108–119 (2015).
51. Crooke, S. T., Witztum, J. L., Bennett, C. F. & Baker, B. F. RNA-Targeted Therapeutics. *Cell Metab* **27**, 714–739 (2018).

52. Schwarz, D. S. *et al.* Asymmetry in the assembly of the RNAi enzyme complex. *Cell* **115**, 199–208 (2003).

53. Meng, Z. & Lu, M. RNA Interference-Induced Innate Immunity, Off-Target Effect, or Immune Adjuvant? *Front Immunol* **8**, 331 (2017).

54. Reynolds, A. *et al.* Induction of the interferon response by siRNA is cell type- and duplex length-dependent. *RNA* **12**, 988–993 (2006).

55. Hornung, V. *et al.* Sequence-specific potent induction of IFN-alpha by short interfering RNA in plasmacytoid dendritic cells through TLR7. *Nat Med* **11**, 263–270 (2005).

56. Dalpke, A. & Helm, M. RNA mediated Toll-like receptor stimulation in health and disease. *RNA Biol* **9**, 828–842 (2012).

57. Choung, S., Kim, Y. J., Kim, S., Park, H.-O. & Choi, Y.-C. Chemical modification of siRNAs to improve serum stability without loss of efficacy. *Biochem Biophys Res Commun* **342**, 919–927 (2006).

58. Behlke, M. A. Chemical modification of siRNAs for in vivo use. *Oligonucleotides* **18**, 305–319 (2008).

59. Hajeri, P. B. & Singh, S. K. siRNAs: their potential as therapeutic agents – Part I. Designing of siRNAs. *Drug Discovery Today* **14**, 851–858 (2009).

60. Sioud, M. Does the understanding of immune activation by RNA predict the design of safe siRNAs? *Front Biosci* **13**, 4379–4392 (2008).

61. Micklefield, J. Backbone modification of nucleic acids: synthesis, structure and therapeutic applications. *Curr Med Chem* **8**, 1157–1179 (2001).

62. Nguyen, D., Zandarashvili, L., White, M. A. & Iwahara, J. Stereospecific Effects of Oxygen-to-Sulfur Substitution in DNA Phosphate on Ion Pair Dynamics and Protein-DNA Affinity. *Chembiochem* **17**, 1636–1642 (2016).

63. Overhoff, M. & Sczakiel, G. Phosphorothioate-stimulated uptake of short interfering RNA by human cells. *EMBO Rep* **6**, 1176–1181 (2005).

64. Stessl, M. *et al.* A proteomic study reveals unspecific apoptosis induction and reduction of glycolytic enzymes by the phosphorothioate antisense oligonucleotide oblimersen in human melanoma cells. *J Proteomics* **72**, 1019–1030 (2009).

65. Chiu, Y.-L. & Rana, T. M. siRNA function in RNAi: a chemical modification analysis. *RNA* **9**, 1034–1048 (2003).

66. Chernikov, I. V., Vlassov, V. V. & Chernolovskaya, E. L. Current Development of siRNA Bioconjugates: From Research to the Clinic. *Front Pharmacol* **10**, 444 (2019).

67. Sioud, M., Furset, G. & Cekaite, L. Suppression of immunostimulatory siRNA-driven innate immune activation by 2'-modified RNAs. *Biochem Biophys Res Commun* **361**, 122–126 (2007).

68. Soutschek, J. *et al.* Therapeutic silencing of an endogenous gene by systemic administration of modified siRNAs. *Nature* **432**, 173–178 (2004).

69. Li, L. & Shen, Y. Overcoming obstacles to develop effective and safe siRNA therapeutics. *Expert Opin Biol Ther* **9**, 609–619 (2009).

70. Chen, P. Y. *et al.* Strand-specific 5'-O-methylation of siRNA duplexes controls guide strand selection and targeting specificity. *RNA* **14**, 263–274 (2008).

71. Foster, D. J. *et al.* Advanced siRNA Designs Further Improve In Vivo Performance of GalNAc-siRNA Conjugates. *Mol Ther* **26**, 708–717 (2018).

72. Turanov, A. A. *et al.* RNAi modulation of placental sFLT1 for the treatment of preeclampsia. *Nat Biotechnol* (2018) doi:10.1038/nbt.4297.

73. Allerson, C. R. *et al.* Fully 2‘-Modified Oligonucleotide Duplexes with Improved in Vitro Potency and Stability Compared to Unmodified Small Interfering RNA. *J. Med. Chem.* **48**, 901–904 (2005).

74. Osborn, M. F. *et al.* Efficient Gene Silencing in Brain Tumors with Hydrophobically Modified siRNAs. *Mol Cancer Ther* **17**, 1251–1258 (2018).

75. Lorenz, C., Hadwiger, P., John, M., Vornlocher, H.-P. & Unverzagt, C. Steroid and lipid conjugates of siRNAs to enhance cellular uptake and gene silencing in liver cells. *Bioorg Med Chem Lett* **14**, 4975–4977 (2004).

76. Guo, S., Huang, F. & Guo, P. Construction of folate-conjugated pRNA of bacteriophage phi29 DNA packaging motor for delivery of chimeric siRNA to nasopharyngeal carcinoma cells. *Gene Ther* **13**, 814–820 (2006).

77. Stein, C. A. *et al.* Efficient gene silencing by delivery of locked nucleic acid antisense oligonucleotides, unassisted by transfection reagents. *Nucleic Acids Res* **38**, e3 (2010).

78. Seth, P. P., Tanowitz, M. & Bennett, C. F. Selective tissue targeting of synthetic nucleic acid drugs. *J Clin Invest* **129**, 915–925 (2019).

79. Springer, A. D. & Dowdy, S. F. GalNAc-siRNA Conjugates: Leading the Way for Delivery of RNAi Therapeutics. *Nucleic Acid Ther* **28**, 109–118 (2018).

80. Prakash, T. P. *et al.* Targeted delivery of antisense oligonucleotides to hepatocytes using triantennary N-acetyl galactosamine improves potency 10-fold in mice. *Nucleic Acids Res* **42**, 8796–8807 (2014).

81. de Paula Brandão, P. R., Titze-de-Almeida, S. S. & Titze-de-Almeida, R. Leading RNA Interference Therapeutics Part 2: Silencing Delta-Aminolevulinic Acid Synthase 1, with a Focus on Givosiran. *Mol Diagn Ther* **24**, 61–68 (2020).

82. Jackson, A. L. & Linsley, P. S. Recognizing and avoiding siRNA off-target effects for target identification and therapeutic application. *Nat Rev Drug Discov* **9**, 57–67 (2010).

83. Kulkarni, J. A. *et al.* On the Formation and Morphology of Lipid Nanoparticles Containing Ionizable Cationic Lipids and siRNA. *ACS Nano* **12**, 4787–4795 (2018).

84. Rozema, D. B. *et al.* Dynamic PolyConjugates for targeted in vivo delivery of siRNA to hepatocytes. *Proc Natl Acad Sci U S A* **104**, 12982–12987 (2007).

85. Yin, H. *et al.* Non-viral vectors for gene-based therapy. *Nat Rev Genet* **15**, 541–555 (2014).

86. Kamerkar, S. *et al.* Exosomes facilitate therapeutic targeting of oncogenic KRAS in pancreatic cancer. *Nature* **546**, 498–503 (2017).

87. El Andaloussi, S., Lakhal, S., Mäger, I. & Wood, M. J. A. Exosomes for targeted siRNA delivery across biological barriers. *Adv Drug Deliv Rev* **65**, 391–397 (2013).

88. Jasinski, D., Haque, F., Binzel, D. W. & Guo, P. Advancement of the Emerging Field of RNA Nanotechnology. *ACS Nano* **11**, 1142–1164 (2017).

89. Chenthamara, D. *et al.* Therapeutic efficacy of nanoparticles and routes of administration. *Biomater Res* **23**, 20 (2019).

90. Zhang, X., Goel, V. & Robbie, G. J. Pharmacokinetics of Patisiran, the First Approved RNA Interference Therapy in Patients With Hereditary Transthyretin-Mediated Amyloidosis. *J Clin Pharmacol* (2019) doi:10.1002/jcph.1553.

91. Hu, B., Weng, Y., Xia, X.-H., Liang, X.-J. & Huang, Y. Clinical advances of siRNA therapeutics. *J Gene Med* **21**, e3097 (2019).

92. Coelho, T. *et al.* Safety and efficacy of RNAi therapy for transthyretin amyloidosis. *N Engl J Med* **369**, 819–829 (2013).

93. Gao, Y., Liu, X.-L. & Li, X.-R. Research progress on siRNA delivery with nonviral carriers. *Int J Nanomedicine* **6**, 1017–1025 (2011).

94. Ghosn, B. *et al.* Efficient gene silencing in lungs and liver using imidazole-modified chitosan as a nanocarrier for small interfering RNA. *Oligonucleotides* **20**, 163–172 (2010).

95. Howard, K. A. *et al.* RNA interference in vitro and in vivo using a novel chitosan/siRNA nanoparticle system. *Mol Ther* **14**, 476–484 (2006).

96. Hu-Lieskovan, S., Heidel, J. D., Bartlett, D. W., Davis, M. E. & Triche, T. J. Sequence-specific knockdown of EWS-FLI1 by targeted, nonviral delivery of small interfering RNA inhibits tumor growth in a murine model of metastatic Ewing's sarcoma. *Cancer Res* **65**, 8984–8992 (2005).

97. Urban-Klein, B., Werth, S., Abuharbeid, S., Czubayko, F. & Aigner, A. RNAi-mediated gene-targeting through systemic application of polyethylenimine (PEI)-complexed siRNA in vivo. *Gene Ther* **12**, 461–466 (2005).

98. Schiffelers, R. M. *et al.* Transporting silence: design of carriers for siRNA to angiogenic endothelium. *J Control Release* **109**, 5–14 (2005).

99. Woodrow, K. A. *et al.* Intravaginal gene silencing using biodegradable polymer nanoparticles densely loaded with small-interfering RNA. *Nat Mater* **8**, 526–533 (2009).

100. Cheng, C. J. & Saltzman, W. M. Enhanced siRNA delivery into cells by exploiting the synergy between targeting ligands and cell-penetrating peptides. *Biomaterials* **32**, 6194–6203 (2011).

101. Zhou, J., Patel, T. R., Fu, M., Bertram, J. P. & Saltzman, W. M. Octa-functional PLGA nanoparticles for targeted and efficient siRNA delivery to tumors. *Biomaterials* **33**, 583–591 (2012).

102. Pereira, D., Ramos, E. & Branco, J. Osteoarthritis. *Acta Med Port* **28**, 99–106 (2015).

103. Turkiewicz, A. *et al.* Current and future impact of osteoarthritis on health care: a population-based study with projections to year 2032. *Osteoarthritis Cartilage* **22**, 1826–1832 (2014).

104. Loeser, R. F. Osteoarthritis year in review 2013: biology. *Osteoarthritis Cartilage* **21**, 1436–1442 (2013).

105. Tanamas, S. *et al.* Does knee malalignment increase the risk of development and progression of knee osteoarthritis? A systematic review. *Arthritis Rheum* **61**, 459–467 (2009).

106. Richette, P. *et al.* Benefits of massive weight loss on symptoms, systemic inflammation and cartilage turnover in obese patients with knee osteoarthritis. *Ann Rheum Dis* **70**, 139–144 (2011).

107. Valdes, A. M. & Spector, T. D. Genetic epidemiology of hip and knee osteoarthritis. *Nat Rev Rheumatol* **7**, 23–32 (2011).

108. Issa, S. N. & Sharma, L. Epidemiology of osteoarthritis: an update. *Curr Rheumatol Rep* **8**, 7–15 (2006).

109. Brophy, R. H., Gray, B. L., Nunley, R. M., Barrack, R. L. & Clohisy, J. C. Total knee arthroplasty after previous knee surgery: expected interval and the effect on patient age. *J Bone Joint Surg Am* **96**, 801–805 (2014).

110. Brown, T. D., Johnston, R. C., Saltzman, C. L., Marsh, J. L. & Buckwalter, J. A. Posttraumatic osteoarthritis: a first estimate of incidence, prevalence, and burden of disease. *J Orthop Trauma* **20**, 739–744 (2006).

111. Katz, J. N. Total joint replacement in osteoarthritis. *Best Pract Res Clin Rheumatol* **20**, 145–153 (2006).

112. Ong, K. L., Runa, M., Lau, E. & Altman, R. D. Cost-of-illness of knee osteoarthritis: potential cost savings by not undergoing arthroplasty within the first 2 years. *Clinicoecon Outcomes Res* **11**, 245–255 (2019).

113. Argoff, C. E. Topical analgesics in the management of acute and chronic pain. *Mayo Clin Proc* **88**, 195–205 (2013).

114. Comparison of an Antiinflammatory Dose of Ibuprofen, an Analgesic Dose of Ibuprofen, and Acetaminophen in the Treatment of Patients with Osteoarthritis of the Knee | NEJM. https://www.nejm.org/doi/full/10.1056/nejm199107113250203.

115. Lanas, A., Tornero, J. & Zamorano, J. L. Assessment of gastrointestinal and cardiovascular risk in patients with osteoarthritis who require NSAIDs: the LOGICA study. *Ann Rheum Dis* **69**, 1453–1458 (2010).

116. Evans, C. H., Kraus, V. B. & Setton, L. A. Progress in intra-articular therapy. *Nat Rev Rheumatol* **10**, 11–22 (2014).

117. Piuzzi, N. S., Midura, R. J., Muschler, G. F. & Hascall, V. C. Intra-articular hyaluronan injections for the treatment of osteoarthritis: perspective for the mechanism of action. *Ther Adv Musculoskelet Dis* **10**, 55–57 (2018).

118. Hochberg, M. C. *et al.* American College of Rheumatology 2012 recommendations for the use of nonpharmacologic and pharmacologic therapies in osteoarthritis of the hand, hip, and knee. *Arthritis Care Res (Hoboken)* **64**, 465–474 (2012).

119. McAlindon, T. E. *et al.* OARSI guidelines for the non-surgical management of knee osteoarthritis. *Osteoarthritis Cartilage* **22**, 363–388 (2014).

120. Wernecke, C., Braun, H. J. & Dragoo, J. L. The Effect of Intra-articular Corticosteroids on Articular Cartilage: A Systematic Review. *Orthop J Sports Med* **3**, 2325967115581163 (2015).

121. McAlindon, T. E. *et al.* Effect of Intra-articular Triamcinolone vs Saline on Knee Cartilage Volume and Pain in Patients With Knee Osteoarthritis: A Randomized Clinical Trial. *JAMA* **317**, 1967–1975 (2017).

122. Larsen, C. *et al.* Intra-articular depot formulation principles: role in the management of postoperative pain and arthritic disorders. *J Pharm Sci* **97**, 4622–4654 (2008).

123. Young, I.-C. *et al.* A novel compressive stress-based osteoarthritis-like chondrocyte system. *Exp Biol Med (Maywood)* **242**, 1062–1071 (2017).

124. Hollander, A. P. *et al.* Damage to type II collagen in aging and osteoarthritis starts at the articular surface, originates around chondrocytes, and extends into the cartilage with progressive degeneration. *J Clin Invest* **96**, 2859–2869 (1995).

125. Yasuda, T. Cartilage destruction by matrix degradation products. *Mod Rheumatol* **16**, 197–205 (2006).

126. Klatt, A. R. *et al.* A critical role for collagen II in cartilage matrix degradation: collagen II induces pro-inflammatory cytokines and MMPs in primary human chondrocytes. *J Orthop Res* **27**, 65–70 (2009).

127. Lee, A. S. *et al.* A current review of molecular mechanisms regarding osteoarthritis and pain. *Gene* **527**, 440–447 (2013).

128. Krzeski, P. *et al.* Development of musculoskeletal toxicity without clear benefit after administration of PG-116800, a matrix metalloproteinase inhibitor, to patients with knee osteoarthritis: a randomized, 12-month, double-blind, placebo-controlled study. *Arthritis Res Ther* **9**, R109 (2007).

129. Settle, S. *et al.* Cartilage degradation biomarkers predict efficacy of a novel, highly selective matrix metalloproteinase 13 inhibitor in a dog model of osteoarthritis: confirmation by multivariate analysis that modulation of type II collagen and aggrecan degradation peptides parallels pathologic changes. *Arthritis Rheum* **62**, 3006–3015 (2010).

130. Liu, J. & Khalil, R. A. Matrix Metalloproteinase Inhibitors as Investigational and Therapeutic Tools in Unrestrained Tissue Remodeling and Pathological Disorders. *Prog Mol Biol Transl Sci* **148**, 355–420 (2017).

131. Cai, H. *et al.* Assessment of the renal toxicity of novel anti-inflammatory compounds using cynomolgus monkey and human kidney cells. *Toxicology* **258**, 56–63 (2009).

132. Jackson, M. A. *et al.* Dual carrier-cargo hydrophobization and charge ratio optimization improve the systemic circulation and safety of zwitterionic nano-polyplexes. *Biomaterials* **192**, 245–259 (2019).

133. Evans, B. C. *et al.* Ex vivo red blood cell hemolysis assay for the evaluation of pH-responsive endosomolytic agents for cytosolic delivery of biomacromolecular drugs. *J Vis Exp* e50166 (2013) doi:10.3791/50166.

134. Kilchrist, K. V. *et al.* Gal8 Visualization of Endosome Disruption Predicts Carrier-Mediated Biologic Drug Intracellular Bioavailability. *ACS Nano* **13**, 1136–1152 (2019).

135. Walkey, C. D., Olsen, J. B., Guo, H., Emili, A. & Chan, W. C. W. Nanoparticle Size and Surface Chemistry Determine Serum Protein Adsorption and Macrophage Uptake. *J. Am. Chem. Soc.* **134**, 2139–2147 (2012).

136. Kelly, I. B., Fletcher, R. B., McBride, J. R., Weiss, S. M. & Duvall, C. L. Tuning Composition of Polymer and Porous Silicon Composite Nanoparticles for Early Endosome Escape of Anti-microRNA Peptide Nucleic Acids. *ACS Appl. Mater. Interfaces* **12**, 39602–39611 (2020).

137. Lv, H., Zhang, S., Wang, B., Cui, S. & Yan, J. Toxicity of cationic lipids and cationic polymers in gene delivery. *Journal of Controlled Release* **114**, 100–109 (2006).

138. Maudens, P., Jordan, O. & Allémann, E. Recent advances in intra-articular drug delivery systems for osteoarthritis therapy. *Drug Discovery Today* **23**, 1761–1775 (2018).

139. Brown, S., Kumar, S. & Sharma, B. Intra-articular targeting of nanomaterials for the treatment of osteoarthritis. *Acta Biomaterialia* **93**, 239–257 (2019).

140. Palmer, A. W., Guldberg, R. E. & Levenston, M. E. Analysis of cartilage matrix fixed charge density and three-dimensional morphology via contrast-enhanced microcomputed tomography. *Proceedings of the National Academy of Sciences* **103**, 19255–19260 (2006).

141. Bajpayee, A. G., Wong, C. R., Bawendi, M. G., Frank, E. H. & Grodzinsky, A. J. Avidin as a model for charge driven transport into cartilage and drug delivery for treating early stage post-traumatic osteoarthritis. *Biomaterials* **35**, 538–549 (2014).

142. Trouvin, A.-P. & Perrot, S. Pain in osteoarthritis. Implications for optimal management. *Joint Bone Spine* **85**, 429–434 (2018).